NASA Contractor Report 4057

Linear Baroclinic Instability in the Presence of Large Scale Topography

Nathaniel Dunton Reynolds

CONTRACT NAS8-36474
MARCH 1987

NASA

NASA Contractor Report 4057

Linear Baroclinic Instability in the Presence of Large Scale Topography

Nathaniel Dunton Reynolds
Universities Space Research Association
Huntsville, Alabama

Prepared for
George C. Marshall Space Flight Center
under Contract NAS8-36474

National Aeronautics
and Space Administration

Scientific and Technical
Information Branch

1987

ACKNOWLEDGEMENTS

I would like to thank Dr. Albert Barcilon for his insight and patience, and for the encouragement he continually gave me throughout this study. I would like to express my appreciation to Dr. Richard L. Pfeffer for his discussions with me concerning the GFDI laboratory experiments, to Dr. Louis N. Howard for fruitful discussions concerning the mathematics, and to Drs. Noel E. LaSeur and James J. O'Brien for helpful comments during this research. I am very grateful to Dr. Timothy L. Miller for the times in which I could discuss with him various ideas concerning this research.

Thanks are due GFDI and the Department of Meteorology at Florida State University for the use of various facilities, including computing facilities, during the early part of my research. I wish to express appreciation to Marshall Space Flight Center and Universities Space Research Association for their support of this work during its latter phases under contracts NAS8-34010 and NAS8-36474, and for the use of computing equipment.

I wish to express my sincere gratitude to my wife, Charlene, for her continual support of my study and the encouragement she has never ceased to offer me.

TABLE OF CONTENTS

LIST OF TABLES

LIST OF FIGURES

LIST OF SYMBOLS

$a_{k\ell n}$	Spectral component of streamfunction associated with zonal wavenumber k, meridional wavenumber ℓ, and layer n
$A_{n\pm}$	Coefficients for the stationary wave solution
$b_{n\pm}$	The y-structure functions for the stationary wave, parameterized as constants
D	Depth of a layer
D_t	Total derivative with respect to time
E_n	Ekman dissipation for layer n
f_0	Coriolis parameter at 45 degrees latitude
F	Internal rotational Froude number
F_e	External rotational Froude number
g	Acceleration of gravity
$g_{n\pm}$	The y-structure function in the layer n for the asymptotic model
h_*	Dimensional topography height
h_0	Nondimensional topography height
H	Depth of model
k	Zonal wavenumber
ℓ	Meridional wavenumber
L	The horizontal length scale, equal to 4500 km
L_D	Rossby deformation radius
N	Brunt-Vaisala frequency

n	Layer designator
p	Nondimensional pressure
p_n	Nondimensional pressure at level n
p_s	Globally averaged pressure at a given height
p_*	Dimensional pressure
$Q_{k\ell n}$	Potential vorticity associated with zonal wavenumber k, meridional wavenumber ℓ, and layer n
$q_n^{s,t}$	Stationary and transient potential vorticity in layer n.
r_n	Dissipative coefficient for layer n
Ro	Rossby number
t	Nondimensional time
t_*	Dimensional time
U	Basic state zonal velocity (nondimensional)
U_*	Dimensional zonal velocity scale
x	Nondimensional eastward Cartesian coordinate
x_*	Dimensional eastward Cartesian coordinate
y	Nondimensional northward Cartesian coordinate
y_*	Dimensional northward Cartesian coordinate
z	Nondimensional vertical Cartesian coordinate
z_*	Dimensional vertical Cartesian coordinate
$\alpha_{n\pm}$	Coefficients in y-structure equation for asymptotic model
β	Nondimensional planetary vorticity gradient
β_0	Dimensional planetary vorticity gradient
γ	Amplitude (complex) of upper layer of baroclinic wave without topography

Γ	Phase lag associated with γ
$\gamma_{n\pm}$	Related to coefficients in stationary wave problem
∂_α	Partial derivative with respect to α
$\Delta^{s,t}$	Amplitudes of stationary and time-dependent waves
∇^2	Horizontal Laplacian
η	Nondimensional topography height variable
θ	Nondimensional potential temperature
θ_s	Globally averaged potential temperature
θ_*	Dimensional potential temperature
$\theta_{n\pm}$	Phase associated with y-structure functions for asymptotic model
θ^s	Phase of stationary wave
$\lambda_{\pm\pm}$	Argument (complex) of trig functions in y-structure functions for asymptotic model
Λ_n	Meridionally-dependent amplitude of order h_0/F modulated wave
ν_n	Eddy diffusivity in layer n
ρ	Nondimensional density
ρ_*	Dimensional density
ρ_s	Globally averaged density
ϕ_n	Perturbation streamfunction in layer n
χ	Phase excursion of wavenumber 2 flow
χ_n	Phase of storm track with respect to domain
ψ_n	Time-Fourier transformed perturbation streamfunction in layer n
ω	Complex frequency

I. INTRODUCTION

Multiple-scale problems are the norm rather than the exception in geophysical flows, and the problem to be described here is of this type. In particular, we consider the scenario consisting of a planetary-scale topography and a baroclinic zonal basic flow for which the most unstable perturbations are synoptic-scale. It has been determined, e.g., by Fredericksen (1979), Blackmon (1976), and Blackmon, et.al. (1977), that in the Earth's atmosphere, there are regions of preferential development of synoptic-scale baroclinic eddies that are dependent on planetary-scale waves. Fig. 1.1 shows the relationship between the Northern Hemisphere oceans and continents, the time-averaged 500mb circulation and bandpass-filtered baroclinic heat-flux data and suggests that the maximum baroclinic heat flux occurs just downstream from the trough axes of the planetery-scale waves, which are located near the eastern edges of the continents. The latitude of maximum heat flux also varies, being closer to the equator near the eastern edges of the continents than further downstream.

In the atmosphere, there are two major forcings by which the planetary-scale waves may arise: a thermal drive, due to land-sea contrasts, and a mechanical drive due to topography.

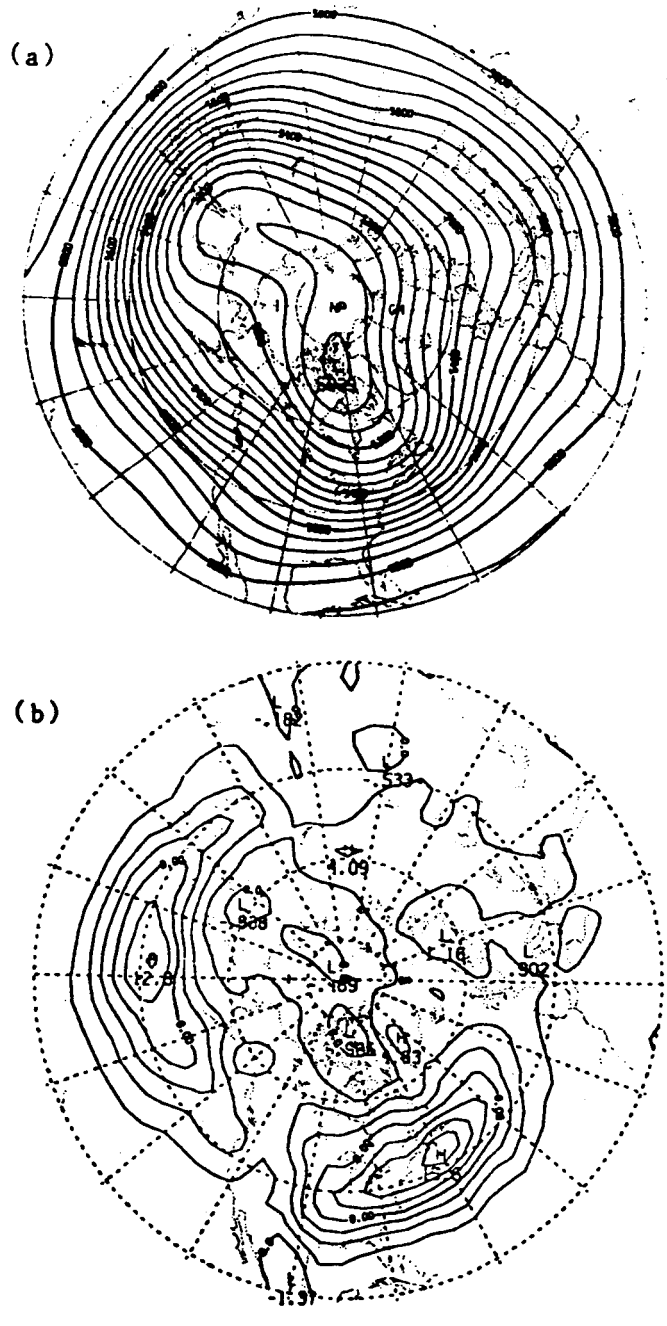

Figure 1.1 a) The 500mb average geopotential height in meters for 9 winters, after Blackmon(1976), and b) the 2-5 day band-pass filtered transient eddy heat flux at 850 mb for this period, after Blackmon, et al. (1977).

Evidence for the importance of topography in maintaining the ultra-long waves is given in Tibaldi and Buzzi (1983); the discussion in this study is limited to the effects of topography.

Early dynamical studies of the effect of topography on a flow field were performed for basic states with no zonal flow at the surface, and only disturbances of a single wavenumber, equal to that of the topography, were considered. These studies have resulted in the discovery of barotropic topographic instability by Charney and DeVore (1979), and Hart (1979), and extensions to baroclinic situations by, e.g. Charney and Straus (1980) and Pedlosky (1981). In the study of Charney and Straus (1980), a severely truncated two-layer spectral model with driving and dissipation yields, among the eigensolutions, a mode which grows in place and other modes which are travelling. The height of the topography must be greater than a critical value for the stationary growing mode to arise. This orographically unstable mode, which draws energy from the zonal flow due to its temperature-phase relationship, is produced by the form drag and therefore Charney and Straus label this instability the "form-drag instability". The travelling modes are of the Eady type modified by topography; i.e., they are present in the limit of no topography, and are called the baroclinic modes.

Pedlosky (1981) solved the problem of a quasi-resonant flow in the presence of topography using weak nonlinearity for both

barotropic and baroclinic flows. Stationary Rossby waves are resonant with a stationary forcing, which is provided by topography through the form drag (Rambaldi, 1982). Pedlosky (1981) considered a flow which is slightly off resonance, in which a very small topography is present. He otherwise did not severely truncate the model, as in Charney and DeVore (1979), or restrict his attention to a strongly anisotropic topography, as in Hart (1979), but proceeded with the analysis valid for a special ordering relationship for topographic height and dissipation in terms of a parameter which is small under quasi-resonant conditions; namely, the speed that a Rossby wave would have if topography were absent. He found that some flows that are baroclinically stable in the absence of topography exhibit topographic instability. The instability can be obtained for arbitrarily small shear, but the width in parameter space of the unstable region is inversely proportional to the shear.

A number of studies have been concerned with the combined baroclinic/topographic problem. A recent example is the study of Nathan (1985), who has extended the model of Pedlosky (1981) by considering a weakly nonlinear problem in which a wavenumber n is orographically unstable and wavenumber n+1 is baroclinically unstable, with comparable growth rates. He demonstrates the importance of internal dissipation in determining the nonlinear evolution of the flow. Attractive features of Nathan's analysis are the explicitness of the dynamical relationships

obtained and the absence of ad-hoc truncation. Two weaknesses of his approach are the requirement for special ordering relations between the topography height and other parameters, and the lack of scale separation between the orographic and baroclinic wavenumbers.

The major purpose of this study is to find the linear response of the model in the presence of baroclinic instability and topography. We will attempt to replicate the parameter settings for the atmosphere, and more particularly, the annulus. We consider the linear baroclinic/orographic instability problem in which the coupling of various wavenumbers by the topography can be significant. In contrast, the topographic effect on the linear problem in the studies of Pedlosky (1981) and Nathan (1985) was not studied explicitly, but brought in at the same order as weakly nonlinear effects. The eigenvalue for our problem is a complex frequency, and the eigenfunction can be approximated by a truncated sum of components of various wavenumbers. Linear investigations of this type of flow have been done by DeSzoeke (1975, 1983) and by Durney (1977) for an infinite f-plane or beta plane, with application to the ocean mesoscale dynamics. Although the atmosphere allows significant meridional wave propagation, we find it useful to consider the case in which the baroclinic instability is confined; hence, we choose a channel domain. The atmospheric studies cited above include a $\sin \pi y$ topography. Our analysis is simplified, in

order to bring out the relevant physical mechanisms, if the topography is independent of the meridional coordinate.

The channel model results also are compared with the results of the recent laboratory experiments of Li, et al (1986), to be referred to hereafter as LKP. Their discussion focuses on an experiment run for a choice of thermal Rossby number and Taylor number for which wave number 6 dominates the flow field when topography is absent. The inclusion of radially-independent, wavenumber 2 topography results in the oscillation of wavenumbers 4 and 6 at a single frequency. Fig. 1.2 also shows a wavenumber 2 disturbance whose phase position of the trough or ridge oscillates from -15 deg to -45 deg and whose amplitude is nearly constant, but exhibiting a frequency twice that of the phase oscillation. The theoretical results to be presented here show a somewhat smaller mean displacement of the trough or ridge and also a somewhat smaller excursion. The tendency for strong cyclones downstream of the topographic ridge, with high pressure dominating upstream of the topography, was also reported by LKP. The results to be presented here are consistent with this finding. The streamfunction fields of LKP are describable kinematically as the sum of a stationary wavenumber 2 component forced by the topography and a travelling disturbance of dominant wavenumber 4, which contains also some wavenumber 2 and wavenumber 6 dependence. The oscillation of the phase of the wavenumber 2 field requires the

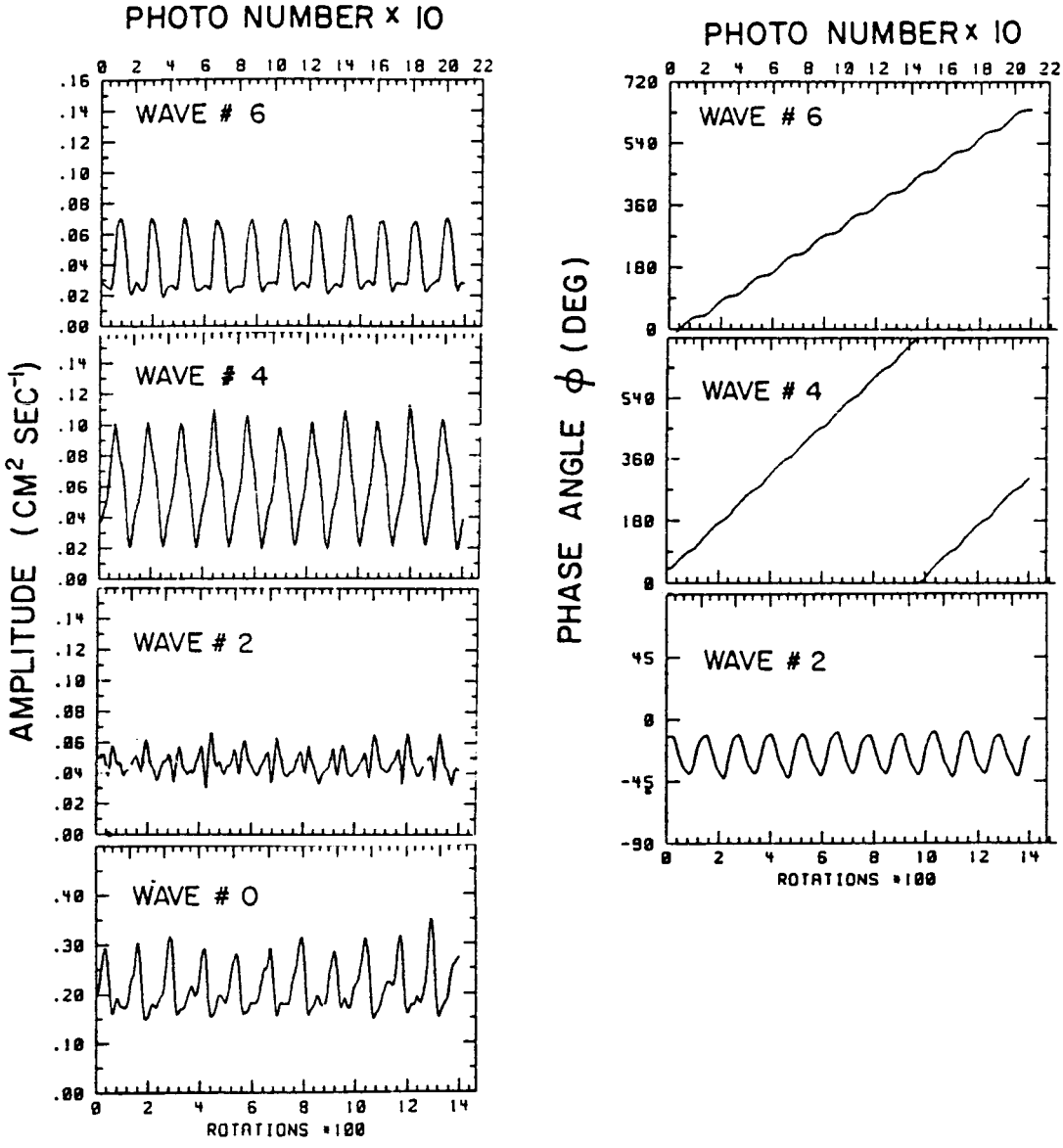

Figure 1.2 Experimental time series of amplitude and phase from rotating annulus experiments with y- independent topography, after Li, et al. (1986).

amplitude of the stationary wave to be larger than the wavenumber 2 component of the travelling wave.

The hypothesis of this study is that the flow field of LKP is the sum of a stationary wavenumber 2 component and a time-dependent wavenumber 4 component. The stationary wavenumber 2 component could result either from topographic forcing due to the presence of a nonzero basic-state zonal velocity at the height of the topography, or it could arise spontaneously due to topographic instability. The latter scenario would require the stationary wave to survive in a finite-amplitude equilibration. No unstable stationary eigenmodes are found for the relevant region in parameter space; hence the model formulation allows for a nonzero zonal velocity in the lower layer, resulting in a stationary forced wave. The time-dependent disturbance observed in the experiments is presumed to be the finite-amplitude equilibration of a single eigenmode of a linear baroclinic problem, whose dominant wavenumber is 4.

In the parameter ranges of relevance to the atmosphere and the experiments of LKP, the topography introduces only a "slight" modification of the time-dependent flow field; hence, this problem can be solved by perturbation methods. The development of the so-called asymptotic model and its results are described in chapter 3. A numerical eigenvalue approach, described in chapter 4, is valid for flows in which the topography effect is larger. The asymptotic model is found to agree

well with the numerical model concerning the growth rate and the spatial structure of the most unstable modes.

The discussion focuses on the hypothesized reconstruction of the flow fields of LKP in terms of the stationary, forced and travelling, free disturbances, and on the comparison of the results of the numerical eigenvalue method with the asymptotic model results.

II. FORMULATION AND STATIONARY WAVE SOLUTION

We used the two-layer quasigeostrophic model to investigate the Boussinesq flow over topography in a beta-plane channel. The problem is formulated for the case of an arbitrary lower-layer basic-state velocity, which induces a forced wave if it is nonzero. The assumption of quasigeostrophy implies that the Rossby number is small. A second small parameter related to the topographic height could be introduced; we take the nondimensional topography height to be of order Rossby number.

The quasi-geostrophic equations are developed in the classical fashion (Pedlosky, 1979; chapter 6). The scaling is as follows:

$$
\begin{aligned}
(x_*, y_*) &= L(x,y), \\
t_* &= L/U_*\ t, \\
z_* &= H\ z, \\
\theta_* &= \theta_s(z)\ (1 + Ro\ F_e\ \theta), \\
p_* &= p_s(z) + \rho_s U_* f_0 L\ p(x,y,z,t), \\
\rho_* &= \rho_s + Ro\ F_e\ \rho(x,y,z,t), \\
\beta &= \beta_0\ L^2/\ U_*,
\end{aligned}
\qquad (2.1)
$$

where * denotes dimensional variables. The channel width is L, and a wavenumber one wavelength is $2\pi L$. The (external) rotational Froude number and the Rossby number are defined by

$$F_e = f_0^2 L^2/gH,$$

$$Ro = U_*/f_0 L \ , \qquad (2.2)$$

and the Coriolis parameter as

$$[f_0 + \beta_0(y_*-L/2)]/f_0 = 1 + Ro\ \beta\ (y-1/2).$$

Dissipation is present in the form of top and bottom Ekman layers, with Ekman numbers given by

$$E_n = 2\ \nu_n/\ f\ H^2 \qquad n=1,2 \qquad (2.3)$$

where ν_n are the eddy diffusivity coefficients. The dissipative coefficients r_n are

$$r_n = E_n^{1/2}/(2\ Ro). \qquad (2.4)$$

We choose our parameters to be of relevance to the atmosphere, as in Table 2.1.

Gates (1961) gives numerical values for $N^2 \sim g\theta^{-1}(\Delta\theta/D)$ for the layer 750 mb to 250 mb, where $D=H/2$ is the depth of a layer. If we average the data from his Table 1 from 1000 mb to 200 mb, we obtain a value for N of .019 (.013) sec^{-1} for the winter (summer). The Rossby deformation radius L_D, given by

$$L_D = ND/f_0, \qquad (2.5)$$

equals 700 km in winter and 570 km in summer. Then the Froude number $F = (L/L_D)^2$ equals 40 in winter and 60 in summer. In the

Table 2.1: Parameter values for the planetary scale

Parameter	Atmospheric Value	Annulus Value
L	4.5×10^6 m	7.5 cm
U_*	10 m sec^{-1}	.14 cm sec^{-1}
H	10^4 m	8.3 cm
D	5×10^3 m	4.2 cm
f_0	10^{-4} sec^{-1}	4.09 sec^{-1}
g	10 m sec^{-2}	10 m sec^{-2}
β_0	2×10^{-11} $m^{-1}sec^{-1}$	0 m^{-1} sec^{-1}

annulus, the Brunt-Vaisala frequency for an imposed 2 deg K temperature difference and with the thermal expansivity coefficient equal to 1.05×10^{-3} (deg K)$^{-1}$ is found to be N = .5 sec^{-1} The resulting deformation radius is about 1 cm, for which F = 56. Since wavenumber 4 is observed to be the dominant wavenumber of the flow with topography, we will consider the case of F=35 for which the minimum critical shear is found at k=4 when topography is absent.

If the Ekman number for the atmosphere is taken to be .001 (.0001), then r_2 is approximately .65 (.2). In the annulus, the Ekman number at the point of interest in parameter space is equal to about 2.2×10^{-4}, yielding $r_2 = 1.5$. The experiments of LKP had a free upper surface, in which case r_2 would be zero. However, for simplicity, we set the upper and lower dissipations equal.

The governing equations, in non-dimensional form, are the conservation of quasi-geostrophic potential vorticity equations in the two layers (Pedlosky (1979), chapter 6),

$$D_t[\nabla^2 p_1 - F(p_1-p_2)+\beta y] = -r_1\nabla^2 p_1,$$
$$D_t[\nabla^2 p_2 - F(p_2-p_1)+\beta y] + J(p_2,\eta) = -r_2\nabla^2 p_2, \qquad (2.6)$$

In eq. (2.6) p_1 and p_2, the pressures at each level, acting as streamfunctions, are of the leading order in Rossby number; the

total time derivative D_t is defined as

$$D_t = \partial_t + p_{nx}\partial_y - p_{ny}\partial_x,$$

with the appropriate value of n being taken in each layer. The (internal) Froude number is defined by

$$F = f_0^2 L^2/N^2 D^2, \tag{2.7}$$

where N is the Brunt-Vaisala frequency, given by

$$N^2 = g\Delta\rho/(\rho D), \tag{2.8}$$

and the nondimensional topography height is defined as

$$\eta = h_*/(H\ Ro). \tag{2.9}$$

In general, η is a function of x and y, but in this study, we shall consider the case of η being a function of x only. The harmonic analysis of the Earth's topography by Peixoto, et al. (1964), points to a dominance of wavenumber 2; however, they find significant contributions by odd wavenumbers as well. In this study we restrict our attention to topography of wavenumber 2; i.e., we write

$$\eta = 2\ h_0\ \cos(2x); \tag{2.10}$$

this choice is motivated, in part, in view of the simplification in the modal interactions and also because the experiments of LKP showed much simpler flow patterns in this case.

The value of h_0 for the annulus using (2.9) and (2.10) is large, on the order of 20. There are several reasons why one might expect the effective topography height to be smaller. The topographic slope should be scaled to the average radius of 11 cm rather than the gap width of 7.5 cm. One could also speculate that cold pools of fluid, decoupled from the rest of the fluid, may sit in the topographic troughs. (Detailed thermal analyses of the experiments of LKP have not been done.) Also, the vortex stretching due to the topography is dependent on the velocity at the surface, which is smaller than U_*. In view of these considerations, it is reasonable to set h_0/F to 1/7; i.e., $h_0 = 5$ for the annulus, a value we will later show to be suggested by the experimental data.

The boundary conditions are given by

$$p_{nx} = \langle p_{nyt} \rangle = 0 \text{ at } y=0,1 \text{ for } n=1,2, \qquad (2.11)$$

where the $\langle\ \rangle$ denote an average over x.

The pressure field is written as a sum of a basic state and a perturbation. The basic state is a westerly current in each layer. We write p_1 and p_2 as

$$p_1 = -U_1 y + \Delta^s \phi_1{}^s + \Delta^t \phi_1{}^t,$$
$$p_2 = -U_2 y + \Delta^s \phi_2{}^s + \Delta^2 \phi_2{}^t, \qquad (2.12)$$

in which there is present a stationary wave, represented by $\phi_n{}^s$ and of scale Δ^s, and a travelling wave represented by $\phi_n{}^t$, whose scale Δ^t is infinitesimal.

Substitution of (2.11) into (2.10) yields the equations

$$[\partial_t + (\Delta^s \phi_{1x}{}^s + \Delta^t \phi_{1x}{}^t)\partial_y + (U_1 - \Delta^s \phi_{1y}{}^s - \Delta^t \phi_{1y}{}^t)\partial_x]$$
$$\{\nabla^2(\Delta^s \phi_1{}^s + \Delta^t \phi_1{}^t) - F[-(U_1 - U_2)y + \Delta^s(\phi_1{}^s - \phi_2{}^s) + \Delta^t(\phi_1{}^t - \phi_2{}^t)] + \beta y\}$$
$$= -r_1 \nabla^2(\Delta^s \phi_1{}^s + \Delta^t \phi_1{}^t), \qquad (2.13)$$

and

$$[\partial_t + (\Delta^s \phi_{2x}{}^s + \Delta^t \phi_{2x}{}^t)\partial_y + (U_2 - \Delta^s \phi_{2y}{}^s - \Delta^t \phi_{2y}{}^t)\partial_x]$$
$$\{\nabla^2(\Delta^s \phi_2{}^s + \Delta^t \phi_2{}^t) - F[-(U_1 - U_2)y + \Delta^s(\phi_2{}^s - \phi_1{}^s) + \Delta^t(\phi_2{}^t - \phi_1{}^t)] + \beta y\}$$
$$+ U_2 \eta_x + J(\Delta^s \phi_2{}^s + \Delta^t \phi_2{}^t, \eta) = -r_1 \nabla^2(\Delta^s \phi_1{}^s + \Delta^t \phi_1{}^t), \qquad (2.14)$$

with

$$\phi_{nx}{}^s = \phi_{nx}{}^t = \langle \phi_{nyt}{}^t \rangle = 0 \text{ at } y = 0,1. \qquad (2.15)$$

The time-independent equations are

$$U_1\partial_x\,[\nabla^2(\phi_1^S)-F(\phi_1^S-\phi_2^S)] + \Delta^S J(\phi_1^S,\nabla^2\phi_1^S-F(\phi_1^S-\phi_2^S)) + \phi_{2x}^S[\beta+F(U_1-U_2)] = -r_1\nabla^2\phi_1^S, \tag{2.16}$$

and

$$U_2\partial_x\,[\nabla^2(\phi_2^S)-F(\phi_2^S-\phi_1^S)] + \Delta^S J(\phi_2^S,\nabla^2\phi_2^S-F(\phi_2^S-\phi_1^S)) + \phi_{2x}^S[\beta-F(U_1-U_2)] + 4U_2/\Delta^S\, h_0 \sin 2x - 4\phi_{2y}^S h_0 \sin 2x = -r_1\nabla^2\phi_1^S, \tag{2.17}$$

with

$$\phi_{nx}^S=0 \text{ at } y = 0,1. \tag{2.18}$$

There is no lateral boundary condition for the zonally-averaged steady flow; however, the specification of the basic-state zonal velocities would imply $\langle\phi_n^S\rangle$ is constant across the domain. Without loss of generality we choose that constant to be zero.

The relative sizes of the terms of equations (2.16) and (2.17) are given in Table 2.2. Term 4 of (2.17) is the forcing, which can balance any of a few other terms. If term 5 is important, then ϕ_2^S is a sum of components of even wavenumbers. A coupling of zonal harmonics also occurs when the nonlinear term 2 is important. We consider the case where terms 3 and 4 balance. We assume that we can ignore term 2 of eq. (2.16) and terms 2 and 5 of eq. (2.17). This assumption, which we shall

Table 2.2: Relative sizes of the terms of equations (2.16) and (2.17), after dividing through by F. Numerical values of terms in (2.17) are given for the case $U_1 = 1$, $U_2 = .3$, $h_0/F = .07$, $r_2/F = .03$ for the atmosphere, and the case $U_1 = 1$, $U_2 = .3$, $h_0/F = .15$, $r_2/F = .03$ for the annulus.

Term	(2.16)	(2.17)	atmosphere	annulus
1.	U_1	U_2	.4	.3
2.	Δ^s	Δ^s	.2	.2
3.	U_1-U_2	U_1-U_2	1	1
4.	r_1/F	$4U_2h_0/(F\Delta^s)$	1	1
5.		$4\ h_0/F$	.4	.6
6.		r_2/F	.02	.025

call Assumption A, is strictly valid only when Δ^S is small. Although r_2/F is small, r_2 is important for determining the phase, which is determined by the relationship between dissipation and advection by the basic-state velocity.

If the stationary wave is written as follows:

$$\Delta^S \phi_n{}^S = (h_0/F)\mathrm{Re}\{b_{n+}(y)\exp(2ix)+b_{n-}(y)\exp(-2ix)\}, \quad (2.19)$$

then we obtain two pairs of equations:

$$\left[\frac{d^2}{dy^2} + \gamma_{1\pm}\right] b_{1\pm} + \gamma_{2\pm}\, b_{2\pm} = 0, \quad (2.20)$$

$$\left[\frac{d^2}{dy^2} + \gamma_{3\pm}\right] b_{2\pm} + \gamma_{4\pm}\, b_{1\pm} = -\gamma_{4\pm}, \quad (2.21)$$

with

$$b_{1\pm} = b_{2\pm} = 0 \quad (2.22)$$

at $y = 0,1$, where

$$\begin{aligned}
\gamma_{1\pm} &= (\beta - FU_2 - 4U_1 \pm 2ir_1)/(U_1 \mp ir_1/2),\\
\gamma_{2\pm} &= U_1 F / (U_1 \mp ir_1/2),\\
\gamma_{3\pm} &= (\beta - FU_1 - 4U_2 \pm 2ir_2)/(U_2 \mp ir_2/2),\\
\gamma_{4\pm} &= U_2 F / (U_2 \mp ir_2/2).
\end{aligned} \quad (2.23)$$

We combine equations (2.20) and (2.21) into a single fourth-order equation:

$$\left[\frac{d^4}{dy^4} + (\gamma_{1\pm}+\gamma_{3\pm}) \frac{d^2}{dy^2} + (\gamma_{1\pm}\gamma_{3\pm}-\gamma_{2\pm}\gamma_{4\pm}) \right] b_{2\pm} = 0, \qquad (2.24)$$

with boundary conditions

$$b_{2\pm} = \left[\frac{d^2}{dy^2} + \gamma_{3\pm} \right] b_{2\pm} + \gamma_{4\pm} = 0 \qquad (2.25)$$

at $y = 0, 1$. The solution is given by

$$\begin{aligned} b_{2+} &= A_{1+} \cos \lambda_{++}(y-1/2) + A_{2+} \cos \lambda_{+-}(y-1/2) + A_{3+}, \\ b_{2-} &= A_{1-} \cos \lambda_{-+}(y-1/2) + A_{2+} \cos \lambda_{--}(y-1/2) + A_{3-}, \end{aligned} \qquad (2.26)$$

where

$$\begin{aligned} \lambda_{++}^2 &= (\gamma_{1+}+\gamma_{3+})/2 + [(\gamma_{1+}-\gamma_{3+})^2/4 + \gamma_{2+}\gamma_{4+}]^{1/2}, \\ \lambda_{+-}^2 &= (\gamma_{1+}+\gamma_{3+})/2 - [(\gamma_{1+}-\gamma_{3+})^2/4 + \gamma_{2+}\gamma_{4+}]^{1/2}, \\ \lambda_{-+}^2 &= (\gamma_{1-}+\gamma_{3-})/2 + [(\gamma_{1-}-\gamma_{3-})^2/4 + \gamma_{2-}\gamma_{4-}]^{1/2}, \\ \lambda_{--}^2 &= (\gamma_{1-}+\gamma_{3-})/2 - [(\gamma_{1-}-\gamma_{3-})^2/4 + \gamma_{2-}\gamma_{4-}]^{1/2}, \end{aligned} \qquad (2.27)$$

and where

$$A_{1+} = (-\gamma_{4+} - A_{3+}\lambda_{+-}^2)/[\cos(\lambda_{++}/2)\ (\lambda_{+-}^2-\lambda_{++}^2)]$$

$$A_{2+} = (A_{3+}\lambda_{+-}^2 + \gamma_{4+})/[\cos(\lambda_{+-}/2)\ (\lambda_{+-}^2-\lambda_{++}^2)],$$

$$A_{1-} = (-\gamma_{4-} - A_{3-}\lambda_{--}^2)/[\cos(\lambda_{-+}/2)\ (\lambda_{--}^2-\lambda_{-+}^2)]$$

$$A_{2-} = (A_{3-}\lambda_{--}^2 + \gamma_{4-})/[\cos(\lambda_{--}/2)\ (\lambda_{--}^2-\lambda_{-+}^2)], \qquad (2.28)$$

and

$$A_{3\pm} = \gamma_{4\pm}\gamma_{1\pm}/(\gamma_{1\pm}\gamma_{3\pm}-\gamma_{2\pm}\gamma_{4\pm}).$$

The plots of $\phi_n^s/(h_0/F)$ for $F = 35$, $r_n = 1.5$, shown in Fig. 2.1, for n equal to 1 and 2, feature an upstream shift of the ridge (trough) of ϕ_n^s from the topographic ridge (trough) positions. The phase shift is -10(-15) degrees for the lower (upper) layers, a somewhat smaller phase shift than the average position of the wavenumber 2 component of LKP. of the wavenumber 2 component in LKP.

The terms in equations (2.13)-(2.15) that are linear in Δ^t yield the following set of equations:

$$[\partial_t+U_1\partial_x]q_1^t+\Delta^s J(\phi_1^s,q_1^t) + \phi_{1x}^t[\beta+F(U_1-U_2)]$$
$$+ \Delta^s J(\phi_1^t,q_1^s) = -r_1\nabla^2\phi_1^t \qquad (2.29)$$

$$[\partial_t+U_2\partial_x]q_2^t+\Delta^s J(\phi_2^s,q_2^t) + \phi_{2x}^t[\beta-F(U_1-U_2)]$$
$$+ \Delta^s J(\phi_2^t,q_2^s) + J(\phi_2^t,\eta) = -r_2\nabla^2\phi_2^t, \qquad (2.30)$$

where stationary and time dependent potential vorticities $q_n^{s,t}$ are defined by

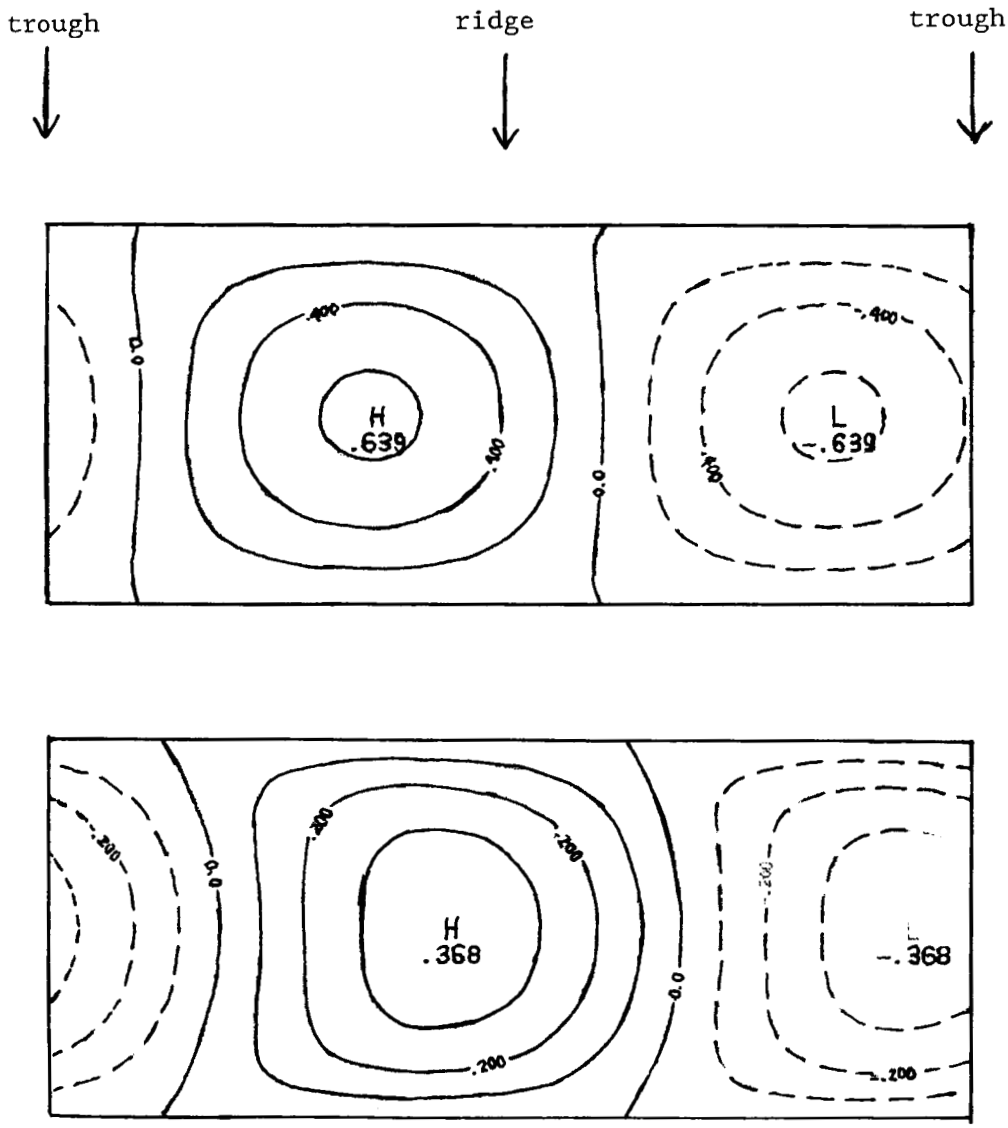

Figure 2.1 The order h_0/F stationary flow of wave number 2 resulting from the interaction of the lower layer basic-state zonal flow with topography, for $U_1=1$, $U_2=.15$, $F=35$, $\beta=0$, and $r_1=r_2=1.5$.

$$q_1^{s,t} = [\nabla^2\phi_1^{s,t} - F(\phi_1^{s,t} - \phi_2^{s,t})]$$
$$q_2^{s,t} = [\nabla^2\phi_2^{s,t} - F(\phi_2^{s,t} - \phi_1^{s,t})]. \qquad (2.31)$$

We define the complex streamfunction amplitude ψ_n^t by

$$\phi_n^t = \mathrm{Re}\{\psi_n \exp(-i\omega t)\}, \qquad (2.32)$$

for n=1,2. The lower velocity U_2 is taken to be order 1, since if U_2 were less than order 1, the amplitude Δ^s of ϕ_n^s would not be large enough to cause the oscillation in the wavenumber 2 phase obtained by LKP. Then, the governing equations and boundary conditions become

$$[(-i\omega+U_1\partial_x)(\nabla^2-F)+r_1\nabla^2+[\beta+F(U_1-U_2)]\partial_x]\psi_1$$
$$+ (h_0/F)\,[J(\phi_1^s,(\nabla^2-F)\psi_1) + J(\psi_1,q_1^s)]$$
$$+ [-i\omega+U_1\partial_x]F\psi_2 + (h_0/F)J(\phi_1^s,\psi_2) = 0, \qquad (2.33)$$

and

$$[(-i\omega+U_2\partial_x)(\nabla^2-F)+r_2 2\nabla^2+[\beta-F(U_1-U_2)]\partial_x]\psi_2$$
$$+ (h_0/F)\,[J(\phi_2^s,(\nabla^2-F)\psi_2) + J(\psi_2,q_2^s)] + J(\psi_2,\eta)$$
$$+ [-i\omega+U_2\partial_x]F\psi_1 + (h_0/F)J(\phi_2^s,\psi_1) = 0, \qquad (2.34)$$

with

$$\psi_{nx}=\langle\psi_{nyt}\rangle=0 \text{ at } y=0,1. \qquad (2.35)$$

It is convenient to eliminate ψ_1 in favor of ψ_2 and obtain a single equation for ψ_2, viz.,

$$\{[(-i\omega+U_2\partial_x)(\nabla^2-F)+r_2\nabla^2+[\beta-F(U_1-U_2]\partial_x + (h_0/F)[J(\phi_{2s},(\nabla^2-F)\cdot)-J(q_2^s,\cdot)]]$$
$$[(-i\omega+U_1\partial_x)(\nabla^2-F)+r_1\nabla^2+[\beta+F(U_1-U_2)]\partial_x + (h_0/F)[J(\phi_1^s,(\nabla^2-F)\cdot-J(q_2^s,\cdot)]] \quad (2.36)$$
$$+ [-i\omega+U_2\partial_x+(h_0/F)J(\phi_2^s,\cdot)]\ [-i\omega+U_1\partial_x+(h_0/F)J(\phi_1^s,\cdot)]F^2\}\ \psi_2$$
$$+ [(-i\omega+U_1\partial_x)(\nabla^2-F)+r_1\nabla^2+[\beta+F(U_1-U_2)]\partial_x$$
$$+(h_0/F)[J(\phi_1^s,(\nabla^2-F)\cdot)-J(\phi_1^s,\cdot)]]\ (h_0/F)4F\sin 2x\ \psi_{2y} = 0$$

with

$$\psi_{nx}-\langle\psi_{nyt}\rangle=0 \qquad \text{at } y=0,1. \quad (2.37)$$

The standing wave complicates the analysis by introducing y-gradients into the equation for ψ_n. If it were not for the boundary conditions, ϕ_n^s would by y-independent. The plots of ϕ_n^s in Fig. 2.1 show the y-gradients to be the largest near the boundary. We parameterize ϕ_n^s by considering it to be independent of y. We take the amplitude of ϕ_n^s to be .9 times the midstream amplitude given by (2.26):

$$\phi_n^s \sim .9\ [b_{n+}(1/2)\exp(2ix) + (b_{n-}(1/2)\exp(-2ix)]. \quad (2.38)$$

The choices of the parameters h_0/F and U_2 for subsequent analysis are obtained using the experimental data. The lower layer velocity scale from the experiments is about .04 cm sec^{-1}. The specified ratio U_2/U_1 is listed in row 1 of Table 2.3. For these specified ratios, the magnitude of $\Delta^s{\phi_2}^s$ is obtained from the stationary wave solution. The terms $\Delta^s{\phi_2}^s$ and $\Delta^t{\phi_2}^t$ are obtained from the observations, and $\Delta^s{\phi_2}^s/(h_0/F))$ is obtained from the stationary wave solution. The upper layer velocity is computed and these quantities are rescaled so that the upper layer velocity is one unit. These rescaled quantities are listed in rows 3-5. The rescaled observed amplitude excursion is shown in row 6. The parameter h_0/F is determined and listed in row 7. The anticipated wavenumber 2 phase oscillation, obtained from the theory, is of order $(h_0/F)\Delta^t{\phi_2}^t$, and is listed in row 8. Note that a comparison of the observed versus theoretical values of the phase oscillation; i.e., rows 6 and 8, would yield agreement for U_2=.15, for which h_0/F is equal to .15.

The excursion in phase, obtained by means of a kinematic addition of a standing and time-dependent wave 2, 4 can be compared with the experimental results shown in Fig. 1.2. If we write

$$\phi_2 = \Delta^s \cos(2x+\theta^s) + \Delta^t(h_0/F)\cos[2x-\omega_r t+\theta_2], \qquad (2.39)$$

then we find that

Table 2.3: The magnitudes of some observed and theoretical quantities as a function of U_2/U_1.

1. U_2/U_1 (specified)	.1	.2	.3	.4	.5
2. $\Delta^s\phi_{2s}/(h_0/F)$ (theor.)	.25	.5	.8	1.1	1.5
3. Rescaled $\Delta^s\phi_{2s}$	.015	.03	.05	.06	.09
4. Rescaled $\Delta^t{\phi_2}^t$	.02	.04	.06	.08	.11
5. Rescaled $\Delta^s\phi_{2s}/(h_0/F)$	.08	.3	.8	1.5	2.5
6. Rescaled transient wavenumber 2 (obs.)	.003	.007	.01	.015	.02
7. Derived h_0/F	.2	.1	.07	.04	.03
8. $h_0/F\ \Delta^t{\phi_2}^t$ (derived)	.004	.004	.004	.003	.003

$$\phi \sim \cos [2x+\chi], \tag{2.40}$$

where χ is given by

$$\chi = -\omega_r t/2 + \tan^{-1} \left[\frac{\Delta^s - \Delta^t(h_0/F)}{\Delta^s - \Delta^t(h_0/F)} \tan (\omega_r t/2) \right]. \tag{2.41}$$

The maximum of tan χ occurs for

$$\tan \chi = \frac{\Delta^t(h_0/F)}{((\Delta^s)^2 - [(\Delta^t(h_0/F)]^2)^{1/2}} \tag{2.42}$$

which is approximately 1/5. This yields a value of χ equal to approximately 11 degrees, which is on the order of 25 percent smaller than the 15 degree excursion illustrated in Fig. 1.2.

III. ASYMPTOTIC MODEL AND RESULTS

We consider the case in which a baroclinic flow is modified by a very small wavenumber 2 topography; i.e., a planetery scale topography. We start with Eqs. (2.23)-(2.25), assuming that the zonal wavenumber of the leading order solution, which represents a synoptic-scale baroclinic wave, is different from 0 or 2. The governing equations are

$$
\begin{aligned}
&\{[(-i\omega+U_1\partial_x)(\nabla^2-F)+(\beta-FU_s)\partial_x+r_1\nabla^2] \\
&-(h_0/F)[\partial_x(\phi_1{}^s\nabla^2-\nabla^2\phi_1{}^s)\partial_y]\}\psi_1 \\
&\quad+[(-i\omega+U_1\partial_x)F+(h_0/F)F\phi_{2x}{}^s\partial_y]\psi_2 = 0, \\
&\{[(-i\omega+U_2\partial_x)(\nabla^2-F)+(\beta-FU)\partial_x+ r_2\nabla^2] \\
&+(h_0/F)[\partial_x(\phi_2{}^s\nabla^2-\nabla^2\phi_2)+4F\sin 2x]\partial_y\}\psi_2 \\
&\quad+[(-i\omega+U_2\partial_x)F + (h_0/F)F\phi_{1x}{}^s\partial_y]\psi_1 = 0,
\end{aligned}
\tag{3.1}
$$

with boundary conditions

$$
\psi_n = \langle\psi_n\rangle_{yt} = 0 \tag{3.2}
$$

at $y = 0, 1$.

We shall use perturbation methods to solve this set of

equations for a small topography. We expand ψ_n and ω in terms of h_0/F; i.e.,

$$\psi_n = \psi_n^{(0)} + (h_0/F)\psi_n^{(1)} + (h_0/F)^2\,\psi_n^{(2)} + \ldots ,$$
$$\omega = \omega^{(0)} + (h_0/F)\omega^{(1)} + (h_0/F)^2\,\omega^{(2)} + \ldots . \qquad (3.3)$$

The streamfunction ψ_n represents a wavy flow at leading order and at order h_0/F. If the wavenumber of the leading order problem is 4, there will be a zonally-averaged flow at order $(h_0/F)^2$. This component does not affect $\omega_{(2)}$, for in the determination of $\omega^{(2)}$, the application of the solvability condition involves a projection onto the baroclinic wave of wavenumber 4.

The leading order problem is the ordinary baroclinic instability problem without topography. For the two-layer Phillips (1954) model, that problem is described in Pedlosky (1979), chapter 7, and is given by Eq. (2.16)-(2.18) with η=0. One can write, in view of the boundary conditions,

$$\psi_n^{(0)} = A_n \exp(ikx)\,\sin \ell\pi y, \qquad n=1,2 \qquad (3.4)$$

which yields a pair of coupled algebraic equations for the amplitudes A_n of the two layers. The simultaneous nontrivial solution of these requires a determinant of the coefficients of A_1 and A_2 to vanish, yielding the dispersion relation:

$$\omega^{(0)} = k[U_2+1/2\{c_+-i\alpha' \pm [c_-^2-2i\alpha c_+ - \alpha'^2 + 4\alpha]^{1/2}\}], \tag{3.5}$$

where

$$\begin{aligned} c_+ &= U_s - 2\beta(K^2+F)/[K^2(K^2+2F)], \\ c_- &= \{U^2K^4(K^4-4F^2)+4\beta^2F^2\}^{1/2}/[K^2(K^2+2F)], \\ K^2 &= k^2 + \ell^2\pi^2, \\ \alpha' &= (K^2+F)(r_1+r_2)/[k(K^2+2F)], \\ \alpha &= \{r_1r_2K^2-ik[r_2(\beta-U_sK^2)+r_1(\beta-FU_s)]\}/[k^2(K^2+2F)], \\ U_s &= U_1 - U_2. \end{aligned} \tag{3.6}$$

Since this is a linear problem, the amplitude is arbitrary and we set $A_2=1$ and $A_1 = \gamma$, where γ is given by

$$\gamma = 1+K^2/F + [r_2iK^2+(\beta-FU_sk]/(F\omega^{(0)}). \tag{3.7}$$

The phase lag Γ between the lower and upper layers is defined by

$$\gamma = |\gamma| \exp\{-i\,\Gamma\}. \tag{3.8}$$

In the case $\beta=0$ and $r_1=r_2=r$, the critical value of U_s; i.e., the value for which the waves are marginal, is given by

$$U_c = (2r/k)\, K/(2F - K^2)^{1/2}, \tag{3.9}$$

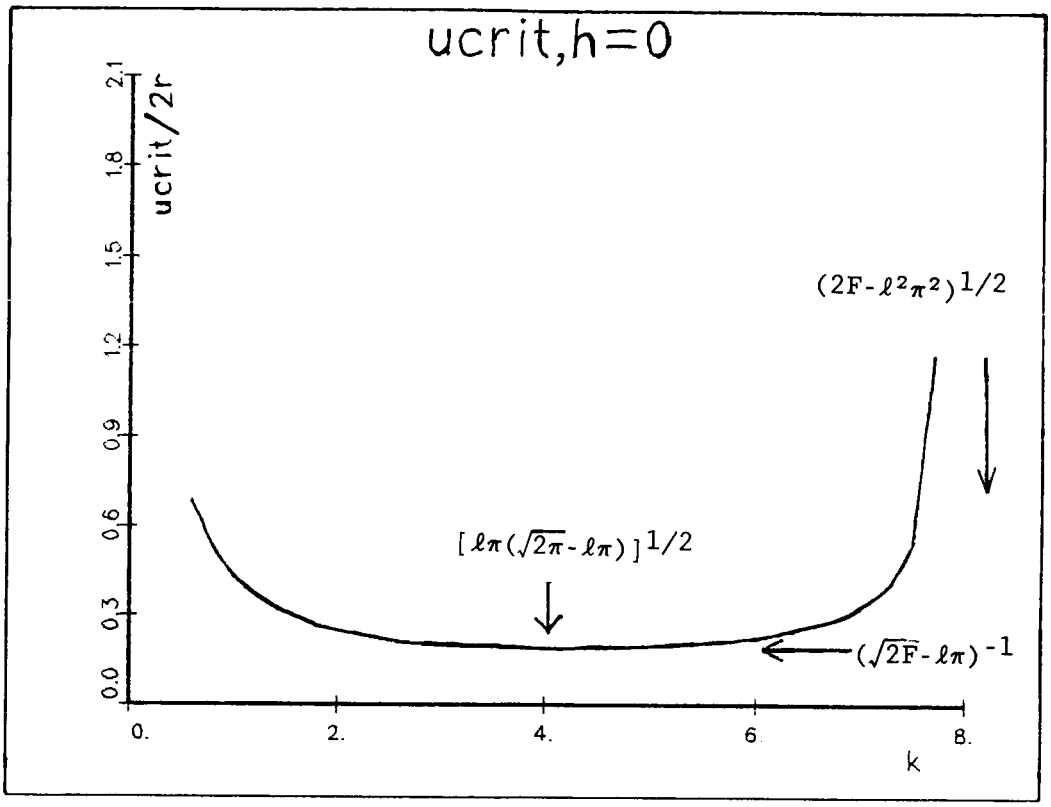

Figure 3.1 The critical shear, $U_c/2r$, as a function of zonal wavenumber, without topography, for F=35 and U_2 = .15. The minimum critical shear and the short wave cutoff are labelled.

for which the square root term in eq. (3.4) balances the negative imaginary term proportional to r that results from the Ekman dissipation. Fig. 3.1 shows a plot of $U_c/2r$ as a function of k, which is valid only if 2F is greater than $\ell^2\pi^2$. If k is greater than $(2F-\ell^2\pi^2)^{1/2}$, no amount of shear will result in an instability. A minimum critical shear of $(\sqrt{(2F)}-\ell\pi)^{-1}$ is realized for $k^2=\ell\pi(\sqrt{(2F)}-\ell\pi)$. For F = 40(60) and ℓ = 1, the minimum critical shear is found at k = 4(5). The positive root in Eq. (3.4) represents a perturbation with a westward tilt of the troughs and ridges with height, as shown in Fig. 3.2 (for t=0, k=5, β=0, F=35, and $r_1 = r_2 = 1.5$), which allows the perturbation to extract energy from the basic state. Marginal stability occurs when dissipation is large enough to balance the energy extracted from the basic state. We select k=4 and ℓ=1 to represent the synoptic-scale wave.

At order h_0/F, we have the governing equations

$$
\begin{aligned}
&-i\omega^{(1)}[\nabla^2-F]\psi_1^{(0)} \; -i\omega^{(1)}F\psi_2^{(0)} \\
&+[(-i\omega^{(0)}+U_1\partial_x)(\nabla^2-F)+r_1\nabla^2+[\beta+F(U_1-U_2)]\partial_x]\psi_1 \\
&\quad + [J(\phi_1^s,(\nabla^2-F)\psi_1^{(0)}) + J(\psi_1^{(0)},q_1^s)] \\
&\quad + [-i\omega^{(0)}+U_1\partial_x]F\psi_2^{(1)} + J(\phi_1^s,\psi_2^{(0)}) = 0,
\end{aligned}
\tag{3.10}
$$

and

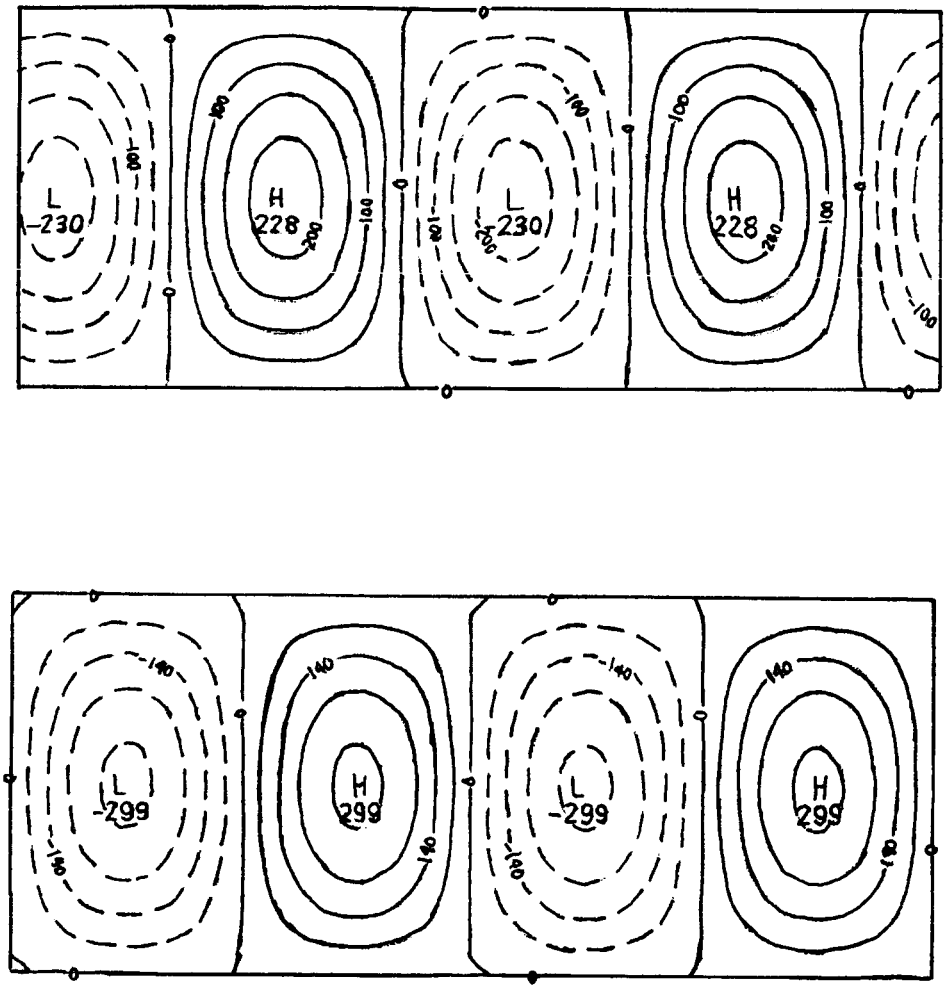

Figure 3.2 The streamfunction for k=5 without topography with $\beta = 0$, $F = 35$, and $r_1 = r_2 = 1.5$, at time t=0, for the two layers, with $U_1 = 1$ and $U_2 = .15$. The region shown is the half-domain $-\pi/2 \le x \le \pi/2$, $0 \le y \le 1$.

$$
\begin{aligned}
&-i\omega^{(1)}[\nabla^2-F]\psi_2^{(0)} - i\omega^{(0)}F\psi_1^{(0)} \\
&+[(-i\omega^{(0)}+U_2\partial_x)(\nabla^2-F)+r_2 2\nabla^2+[\beta-F(U_1-U_2)]\partial_x]\psi_2 \\
&+ [J(\phi_2^s,(\nabla^2-F)\psi_2^{(0)}) + J(\psi_2^{(0)},q_2^s)] + \psi_{2y}^{(0)}\sin 2x \\
&+ [-i\omega^{(0)}+U_2\partial_x]F\psi_1^{(1)} + J(\phi_2^s,\psi_1^{(0)}) = 0,
\end{aligned}
\tag{3.11}
$$

with

$$
\psi_{nx}^{(1)}=\langle\psi_{nyt}^{(1)}\rangle=0 \tag{3.12}
$$

at y=0,1.

The order h_0/F governing equations are composed of three terms: 1) the leading order operators acting on the perturbation $\psi_2^{(1)}$, 2) the order h_0/F operators acting on $\psi_2^{(0)}$, which is proportional to the order h_0/F eigenvalue correction, and 3) the order h_0/F operators due to the topography and the standing wave, which act on the leading order solution.

In order to find $\omega^{(1)}$, we apply a solvability condition; specifically, that any solution to this equation must be orthogonal to the adjoint of the solution of the leading order problem. One can see intuitively, and it is shown formally in Appendix A, that $\omega^{(1)}$ is zero, since the replacement of h_0 by $-h_0$ in the equations merely shifts the phase of the topography by 180 degrees.

With $\omega^{(1)} = 0$, after combining Eqs. (3.10) and (3.11) into a single equation, we obtain a forced equation for $\psi_2^{(1)}$, and the solution $\psi_2^{(1)}$ has the form

$$\psi_2^{(1)} = g_{2+}(y)\exp(i(k+2)x) + g_{2-}(y)\exp(i(k-2)x). \qquad (3.13)$$

One can solve for $g_{2\pm}$ by substituting $\partial_x \sim i(k\pm2)$ into (3.10) and (3.11), solving in terms of the lower-layer streamfunction, and obtaining a pair of fourth-order ordinary differential equations in y:

$$\frac{d^4 g_{2\pm}}{dy^4} + \alpha_{1\pm}\frac{d^2 g_{2\pm}}{dy^2} + \alpha_{2\pm} g_{2\pm} = \alpha_{3\pm} \cos \ell\pi y, \qquad (3.14)$$

with boundary conditions

$$g_{2\pm} = \frac{d^2 g_{2\pm}}{dy^2} + \alpha_{4\pm} g_{2\pm} - (-1)^{\ell}\alpha_{5\pm} = 0 \qquad (3.15)$$

at y = 0,1, where the coefficients $\alpha_{n\pm}$ are defined as

$$\begin{aligned}
\alpha_{1\pm} = -\{&[(\omega^{(0)} - U_2 k)[(k\pm2)^2+F] + r_2 i(k\pm2)^2 + (k\pm2)(\beta - FU_s)\} \\
&/(\omega^{(0)} - U_2(k\pm2) + r_2 i) \\
&- \{[\omega^{(0)} - U_1(k\pm2)][(k\pm2)^2+F] + r_1 i(k\pm2)^2 \\
&+ (k\pm2)(\beta + FU_s)\}/(\omega^{(0)} - U_1(k\pm2) + r_1 i),
\end{aligned}$$

$$\begin{aligned}
\alpha_{2\pm} = [&\{[\omega^{(0)} - U_1(k\pm2)][(k\pm2)^2+F] + (k\pm2)(\beta + FU_s) + r_1(k\pm2)^2 i\} \\
&\cdot\{(\omega^{(0)} - U_2 k)[(k\pm2)^2+F] + (k\pm2)(\beta - FU_s) + r_2 i(k\pm2)^2\} \\
&- \{\omega^{(0)} - U_2(k\pm2)\}\{\omega^{(0)} - U_1(k\pm2)\}F^2] \\
&/[\{\omega^{(0)} - U_1(k\pm2) + r_1 i\}\{\omega^{(0)} + r_2 i\}],
\end{aligned}$$

$$\alpha_{3\pm} = \pm 2\ell\pi[F\{[\omega^{(0)}-U_1(k\pm 2)][(k\pm 2)^2+\ell^2\pi^2+F]+(k\pm 2)(\beta+FU_s)$$
$$+r_1 i[(k\pm 2)^2+\ell^2\pi^2]\}+(k^2+\ell^2\pi^2-4-\gamma F)b_{2+}+Fb_{1+}]$$
$$/\{[\omega^{(0)}-U(k\pm 2)+r_1 i][\omega^{(0)}+r_2 i]\},$$
$$\alpha_{4\pm} = -\{[\omega^{(0)}-U_2(k\pm 2)][(k\pm 2)^2+F]+r_2 i(k\pm 2)^2+(\beta-FU_s)(k\pm 2)\}$$
$$/\{\omega^{(0)}-U_2(k\pm 2)+r_2 i\},$$
$$\alpha_{5\pm} = \mp 2\pi\ell[(4-K^2+\gamma F)b_{2\pm}-F(b_{1\pm}+1)]$$
$$/[\omega^{(0)}-U_2(k\pm 2)+r_2 i]. \qquad (3.16)$$

The solutions to these fourth-order ODE's are given by

$$g_{2+} = a_{1+}\cos\lambda_{++}(y-1/2) + a_{2+}\sin\lambda_{+-}(y-1/2)$$
$$+ a_{3+}\cos\lambda_{+-}(y-1/2) + a_{4+}\sin\lambda_{+-}(y-1/2)$$
$$+ a_{5+}\cos\ell\pi y,$$

$$g_{2-} = a_{1-}\cos\lambda_{-+}(y-1/2) + a_{2-}\sin\lambda_{--}(y-1/2)$$
$$+ a_{3-}\cos\lambda_{--}(y-1/2) + a_{4-}\sin\lambda_{--}(y-1/2)$$
$$+ a_{5-}\cos\ell\pi y, \qquad (3.17)$$

where the $a_{n\pm}$ are constants which must be determined and the λ's are roots of the characteristic quartic equation, which can be found as:

$$\lambda_{++}^2 = \alpha_{1+}/2 + [\alpha_{1+}^2/4 - \alpha_{2+}]^{1/2}$$
$$\lambda_{+-}^2 = \alpha_{1+}/2 - [\alpha_{1+}^2/4 - \alpha_{2+}]^{1/2} \qquad (3.18)$$
$$\lambda_{-+}^2 = \alpha_{1-}/2 + [\alpha_{1-}^2/4 - \alpha_{2-}]^{1/2}$$
$$\lambda_{--}^2 = \alpha_{1-}/2 - [\alpha_{1-}^2/4 - \alpha_{2-}]^{1/2} ,$$

We can find $g_{1\pm}$ from $g_{2\pm}$ by substituting into the lower layer governing equation (2.17).

The functions g_{n+} and g_{n-} are symmetric about $y = 1/2$, which requires that $a_{1+} = a_{1-} = a_{3+} = a_{3-} = 0$ for ℓ odd and $a_{2+} = a_{2-} = a_{4+} = a_{4-} = 0$ for ℓ even. The specific details of the coefficients $a_{n\pm}$ are given in Appendix B.

The time-dependent streamfunction field $\psi_n^{(1)}$ (x,y) is a superposition of Fourier components of zonal wavenumber k±2. A plot is given in Fig. (3.3) for k=5, ℓ=1, for $0 \le x \le \pi$; i.e., for one "period" for the topography. The functions $g_{2\pm}$ have a node at $y = 1/2$, because $\psi_{2y}^{(0)} = 0$ there.

It is instructive to write the functions $g_{n\pm}$'s as

$$g_{n\pm}(y) = G_{n\pm}(y) \exp\{i\, \theta_{n\pm}(y)\}. \qquad (3.19)$$

It was found that $\theta_{n\pm}$ are nearly independent of y, varying approximately $.05\pi$ across the y-domain. The upper and lower streamfunctions ϕ_1 and ϕ_2 are constructed to order h_0/F and are given by

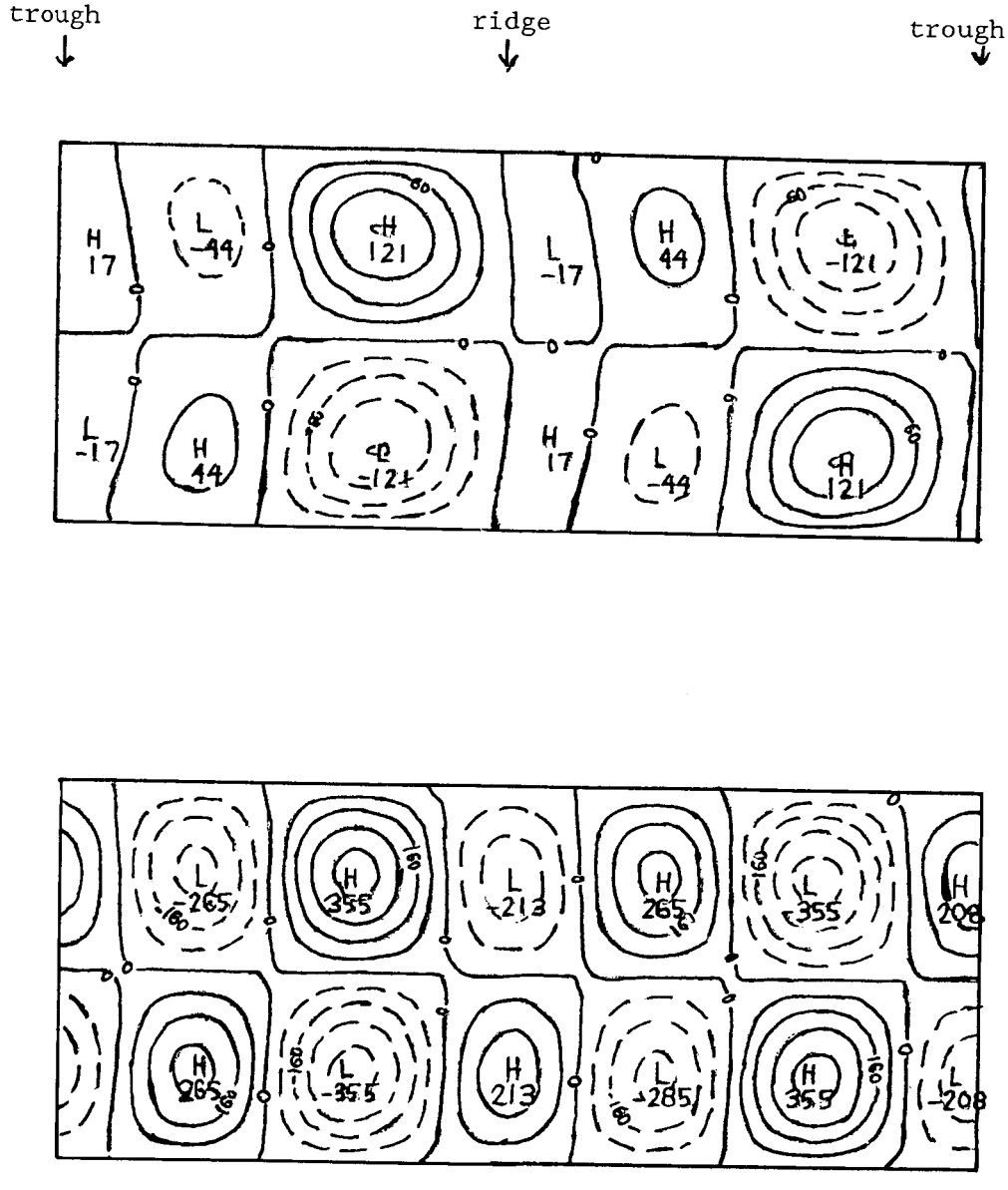

Figure 3.3 The order h_0/F portion of the transient flow, for $h_0 = 5$ and parameters otherwise as given in Fig. 3.2. Positions of the topographic trough and ridge are shown.

$$\phi_1 = \exp(\omega_i t)\{\sin \ell\pi y \cos(kx-\omega_r t-\Gamma) + h_0/F\ G_{1+}(y)\cos[(k+2)x-\omega_r t+\theta_{1+}] + h_0/F\ G_{1-}(y)\cos[(k-2)x-\omega_r t+\theta_{1-}]\},$$

$$\phi_2 = \exp(\omega_i t)\{\sin \ell\pi y \cos(kx-\omega_r t) + h_0/F\ G_{2+}(y)\cos[(k+2)x-\omega_r t+\theta_{2+}] + h_0/F\ G_{2-}(y)\cos[(k-2)x-\omega_r t+\theta_{2-}]\}, \quad (3.20)$$

where $\omega^{(0)} \equiv \omega_r + i\ \omega_i$.

It is useful to write the order h_0 flow as a propagating wave of wavenumber k that is modulated by a standing wavenumber 2 pattern. Then,up to order h_0/F, the total flow field at a fixed latitude can be viewed as an interference pattern between the order 1 and order h_0 flow. The upper streamfunction ϕ_2 is written as

$$\phi_1 = \cos(kx-\omega_r t-\Gamma)\ \exp[\omega_i t]\{\sin\ell\pi y + h_0/F\ \Lambda_1(y)\ \cos[2x-\chi_1(y)]\} + h_0/F\ \sin(kx-\omega_r t - \Gamma)\ \exp[\omega_i t]\ \Lambda_1(y)\ \sin[2x-\chi_1(y)], \quad (3.21)$$

where

$$\Lambda_1 \equiv [G_{1+}^2+G_{1-}^2+2G_{1+}G_{1-}\cos(\theta_{1+}+\theta_{1-}-\Gamma)]^{1/2}, \quad (3.22)$$

and

$$\chi_1 \equiv \left[\frac{\theta_{1+}-\theta_{1-}}{2}\right] - \tan\left\{\frac{(G_{1+}-G_{1-})}{(G_{1+}+G_{1-})}\ \tan\left[\frac{\theta_{1+}+\theta_{1-}}{2}\right]\right\}. \quad (3.23)$$

and where Γ is defined in eq. (3.8). Likewise, the lower layer streamfunction is given by

$$\phi_2 = \cos(kx-\omega_r t)\exp[\omega_i t]\{\sin\ell\pi y + h_0/F\,\Lambda_2(y)\cos[2x-\chi_2(y)]\} + h_0/F\sin(kx-\omega_r t)\exp[\omega_i t]\,\Lambda_2(y)\sin[2x-\chi_2(y)] \tag{3.24}$$

where

$$\Lambda_2 = [G_{2+}^2+G_{2-}^2+2G_{2+}G_{2-}\cos(\theta_{1+}+\theta_{1-})]^{1/2}, \tag{3.25}$$

and

$$\chi_2 = \left[\frac{\theta_{2+}-\theta_{2-}}{2}\right] - \tan\left\{\frac{(G_{2+}-G_{2-})}{(G_{2+}+G_{2-})}\tan\left[\frac{\theta_{2+}+\theta_{2-}}{2}\right]\right\}. \tag{3.26}$$

At longitude $2x = \chi_n$, the order h_0 flow in layer n adds constructively to the order 1 flow, and at longitude $2x = \chi_n+\pi$ is found a destructive interference. Since the order h_0 streamfunction is antisymmetric for $\ell = 1$, the interference pattern for the south half-domain $0\le y<1/2$ is shifted by $\pi/2$ from the north half-domain $1/2<y\le 1$. The functions Λ_n and χ_n are plotted in Fig. 3.4. On each side of the mid-channel latitude, the function χ_n is nearly independent of y. The lower layer amplitude Λ_2 is a maximum at y=1/4 and y=3/4, and the upper layer amplitude maximum is slightly further from the mid-channel.

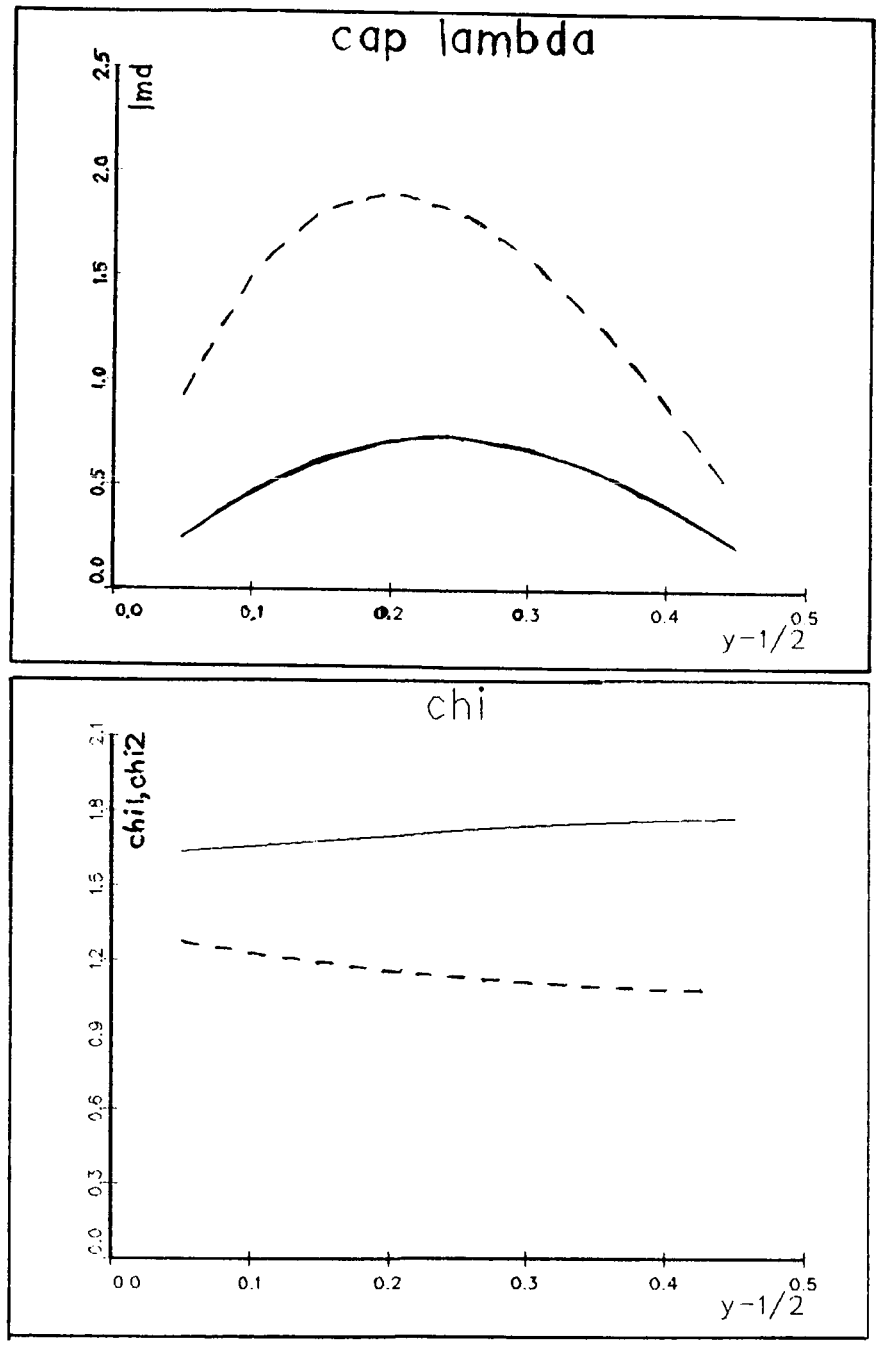

Figure 3.4 Amplitude (Λ_n) and phase (χ_n) of constructive interference between order 1 and order h_0/F solutions, for layers n=1 and n=2, as a function of y - 1/2. For $0<y<1/2$, we note $\Lambda_n(1/2-y) = \Lambda_N(1/2+y)$ and $\chi_n(1/2-y) = \chi_n(1/2+y) \pm\pi$.

The total time-dependent flow field, shown in Fig. 3.5 for times $\omega_r t = 0$, $\pi/2$, π, and $3\pi/2$, is a procession of highs and lows whose centers meander as they move east, on a track whose position is constant in time. For the lower layer, the furthest south excursion is found at about $x=\pi/3$ and the furthest north excursion is found at about $x=-\pi/6$. The amplitude is smaller for the upper layer, and the furthest north excursion is slightly upstream of the topography ridge, and the furthest south excursion near the trough.

One might interpret the avoidance of the low latitudes near $x = -\pi/6$ as the presence of a "blocking ridge", immediately upstream of the topography ridge. This feature of the results is similar to those of LKP. However, LKP found also a strong longitudinal dependence of the strength of the highs and lows; only a weak variation in strength was found for the time-dependent solution alone. The addition of the stationary wave yields a stronger longitude dependence in the amplitude of the wave.

In the atmosphere, Fig. 1.1b, after Blackmon et al. (1977), suggests that the main storm track in winter is further north upstream of the continents than it is downstream. Although the relationship between the path of the cyclones and anticyclones, the eddy heat flux, and the time-mean circulation was noted in the Introduction, it is interesting that the storm track is very evident in Figs. 3.5 and 4.3, while there is very little

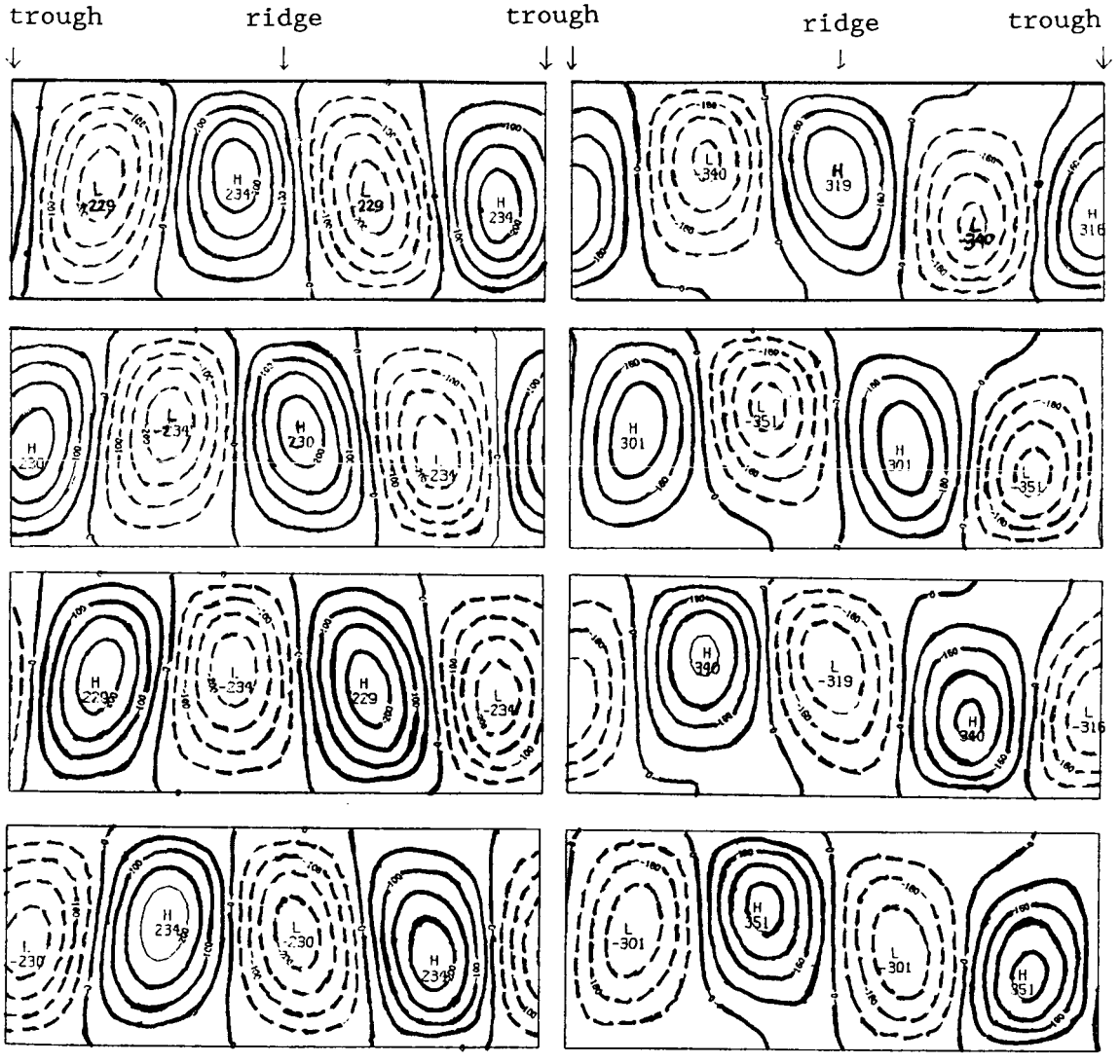

Figure 3.5 The streamfunction ϕ_n^t for layers n=1,2, computed for times $\omega_r t = 0, \pi/2, \pi,$ and $3\pi/2$, using the asymptotic model. Only the half of the domain $-\pi/2 \leq x \leq \pi/2$ is shown. Topographic ridge and trough positions are shown by arrows.

longitude dependence of the intensity of the waves, and the most unstable mode, divided by the exponential growth factor, has a zero time mean; i.e. the time-averaged circulation is simply the zonal basic state. We have demonstrated the possibility that storms follow a meandering path without the presence of a wave in the time-mean circulation.

At order $(h_0/F)^2$ we find the lowest order eigenvalue correction, which is given for the case of $U_2 = 0$ by

$$\omega^{(2)}_I = I' + 4\pi^2 \ell [\omega^{(0)} - Uk + ir_1][\cos \ell\pi y \ (g_{-y} - g_{+y})]\Big|_{y=0}^{y=1}, \tag{3.27}$$

where I and I' are integrals given in Appendix A. The results for arbitrary U_2 are also given in Appendix A. These integrals are obtained by writing the order $(h_0/F)^2$ equations and applying the solvability condition, for obtaining an expression for $\omega^{(2)}$. The streamfunction $\psi_n^{(2)}$ at that order has components of wavenumber k, k+4, and k-4; only the component of wavenumber k contributes.

The marginal stability curve was computed from this small topography perturbation analysis by choosing F and finding the critical dissipation U_c using a Newton's iterative method. A quantity ΔU_c which is the percent difference between U_c for topography height $h_0 = 5$ and U_c for no topography is plotted

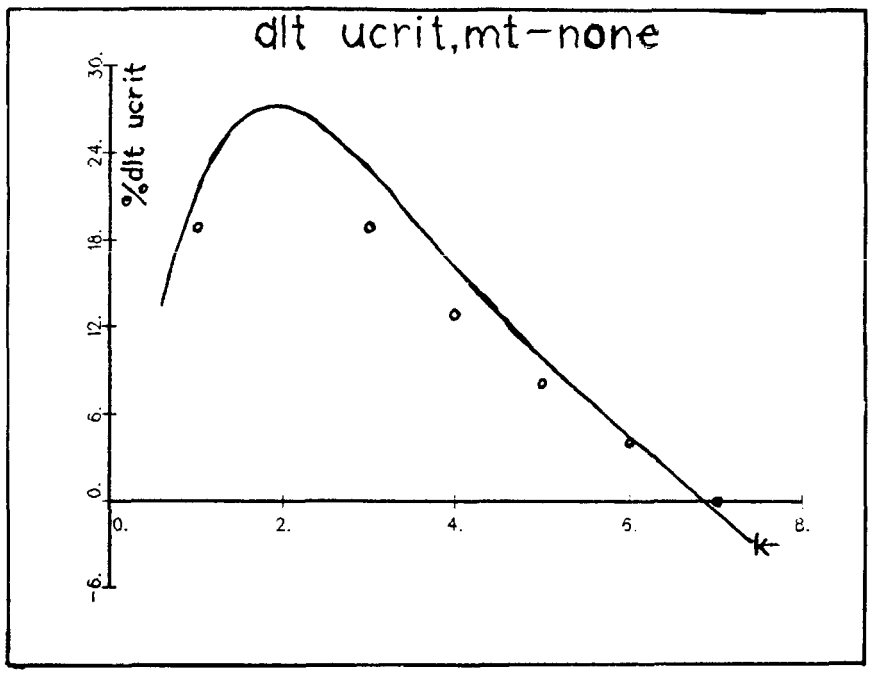

Figure 3.6 The percent change in the critical shear U_c as a function of dominant wavenumber k due to the presence of topography, with F = 35, β = 0, $r_1 = r_2 = 1.5$, and $h_0 = 5$. The solid curve is computed using the asymptotic model, while the circles are obtained from the numerical. No data is obtained at x=2 since the asymptotic model results are invalid there.

as a function of k in Fig. 3.6, for a fixed F = 35. A negative ΔU_c implies destabilization. It can be seen in Fig. 3.6 that the topography destabilizes the flow near the short-wave cutoff for each given wavenumber.

The time-dependent equilibrated amplitude was chosen to be equal to .025, the magnitude the rescaled $\Delta^t\phi_2{}^t$ term from table 2.3 would be when U_2/U_1 is equal to .15.

The sum of the time-dependent field and the stationary wave field, shown in Figure 3.7, reveals a prominent standing wave of wavenumber 2, with a less prominent wavenumber 4 pattern superimposed on it. The combination of the topography and the parameterized standing wave acts as an effective y-independent topography in both layers. Physically the meandering of the storm tracks is a result of the antisymmetry of the vortex stretching about the middle of the channel due to the interaction of the effective topography with the u-velocities associated with the leading-order disturbance. The antisymmetry is masked in the total wave field due to the presence of the larger stationary wave.

A tendency toward high pressure immediately upstream of the topographic ridge and low pressure downstream is evident after the addition of the stationary wave component. The phase of this feature relative to the topography agrees qualitatively with the similar features of the atmosphere and the laboratory experiments.

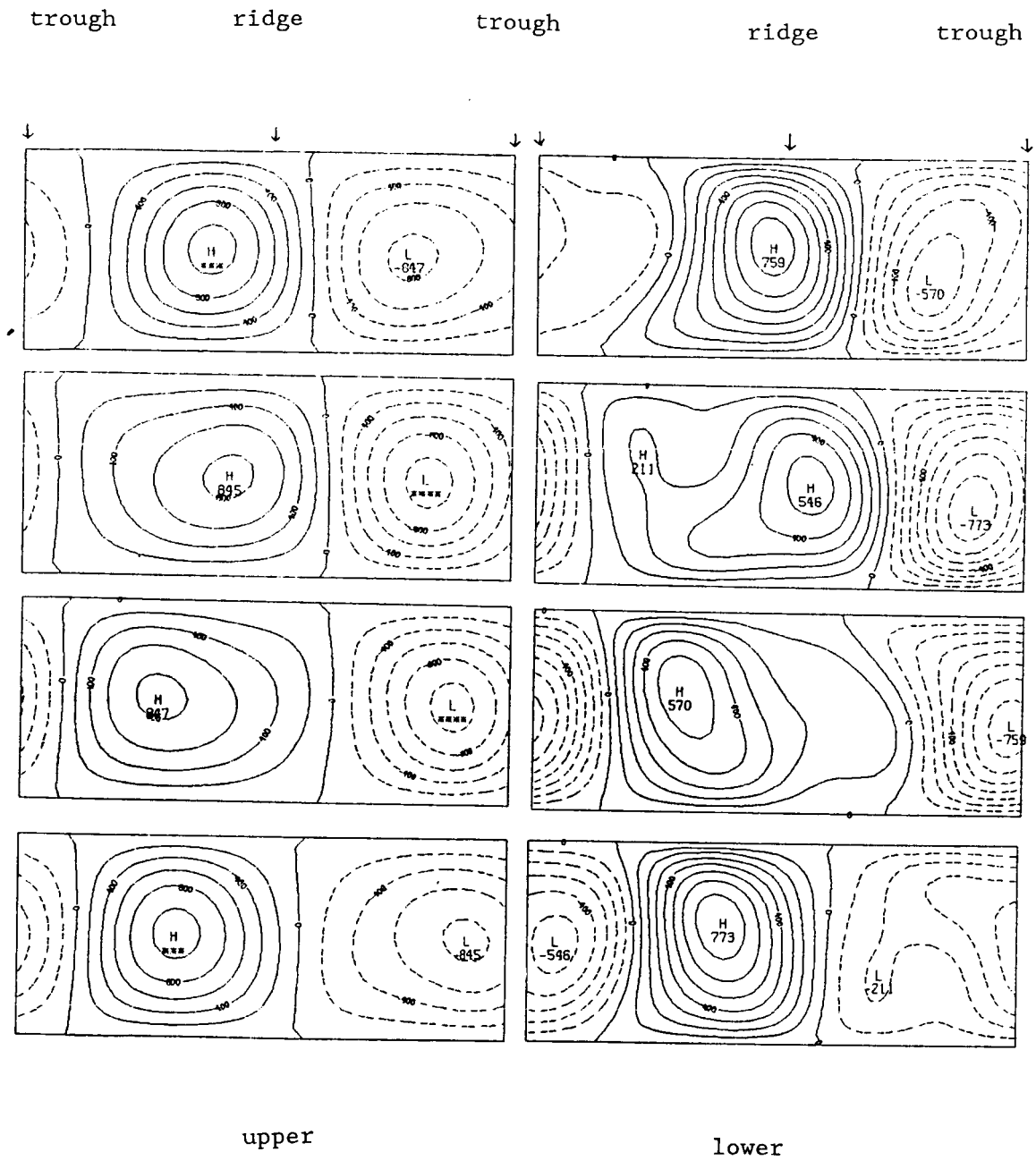

Figure 3.7 The wave streamfunction field, including both the time-dependent and stationary flow fields for various times as in Fig. 3.5.

The antisymmetry of the wavenumber 2 time-dependent solution about the middle of the channel yields a difficulty in the interpretation of the phase oscillation of the wavenumber 2 component. According to the theory presented here, the phase oscillation should be zero at the middle radius and a maximum at y=.25 and y=.75. The observed magnitude of the phase oscillation is nearly independent of the radius. Some of the simplifications in the theory, for example the lack of a stationary wavenumber 4 component and the parameterization of the stationary wave solution may be responsible for this discrepancy.

IV. NUMERICAL APPROACH AND RESULTS

4.1 Formulation:

More general results, i.e., results which are still obtained from a truncated model but one in which we relax some of the smallness restriction on h_0, can be found by numerical methods. The numerical approach in this study was used only for the time-dependent problem. The parameterized stationary wave solution, forced by the topography in the presence of U_2, defines a coupling of the various Fourier components in a manner similar to the topography term. In contrast, many other studies, for example, Pedlosky (1981), consider only a zero lower layer basic state velocity. We use Assumption A described in Chapter 2; namely, assuming the stationary wave parameterization to be valid for arbitrary h_0/F. In this study the main purpose of the numerical approach is for comparison with and validation of the asymptotic time-dependent model results presented in Chapter 3.

We define ψ_n as

$$\psi_n = \sum_{\ell=1}^{\infty} \{a_{0\ell n} \cos \ell\pi y + \sum_{k=-\infty}^{\infty} \exp(ikx)\, a_{k\ell n} \sin \ell\pi y\} \qquad (4.1)$$

and we recall that

$$\eta_x = -\,4\,h_0 \sin 2x. \tag{4.2}$$

We substitute the above expressions into eqs (2.20) and get for the zonally-averaged flow the following equations,

$$\begin{aligned}
&\omega\,[(\ell^2\pi^2+F)a_{0\ell 1} - Fa_{0\ell 2}] + ir_1\ell^2\pi^2\, a_{0\ell 1} \\
&+2\pi\ell(h_0/F)\{b_{1+}[-(2^2+\ell^2\pi^2)a_{-2\ell 1}+Fa_{2\ell 2}] \\
&\quad -b_{1-}[(2^2+\ell^2\pi^2)a_{2\ell 1}+Fa_{2\ell 2}] \\
&\quad +[(4+F)b_{1+}-Fb_{2+}]a_{-2\ell 1} + [(4+F)b_{1-}-Fb_{2-}]a_{2\ell 1}] = 0,
\end{aligned}$$

$$\begin{aligned}
&\omega\,[(\ell^2\pi^2+F)a_{0\ell 2} - Fa_{0\ell 1}] + ir_2\ell^2\pi^2\, a_{0\ell 2} \\
&+2\pi\ell(h_0/F)\{b_{2+}[(-2^2+\ell^2\pi^2)a_{-2\ell 2}+Fa_{2\ell 1}] \\
&\quad -b_{2-}[(2^2+\ell^2\pi^2)a_{2\ell 2}+Fa_{2\ell 1}] \\
&\quad +[(4+F)b_{2+}-Fb_{1+}]a_{-2\ell 2} + [(4+F)b_{2-}-Fb_{1-}]a_{2\ell 2}] = 0 \\
&\qquad + 2\ell\pi h_0[a_{2\ell 2}-a_{-2\ell 2}] = 0,
\end{aligned}$$

and for each zonal nonzero wavenumber k, we obtain the following equations:

$$[(\omega-U_1k)(K^2+F)+k(\beta+FU_s)+irK^2]a_{k\ell 1} - (\omega-U_1k)Fa_{k\ell 2}$$

$$+2\pi\ell h_0/F\{\delta_{k,2}[b_{1+}[-(K_{\ell-}{}^2+F)a_{(k-2)\ell 2}+Fa_{(k-2)\ell 1}]$$

$$+[-(4+F)b_{1+}+Fb_{2+}]a_{(k-2)\ell 1}]]$$

$$-\delta_{k,-2}[b_{1-}[-(K_{\ell+}{}^2+F)a_{(k+2)\ell 2}+Fa_{(k-2)\ell 1}]$$

$$+[-(4+F)b_{1-}+Fb_{2-}]a_{(k+2)\ell 1}]]$$

$$+2\ell\pi h_0\sum_{\ell=1}^{\ell max}[\rho_{m\ell}\{$$

$$(1-\delta_{k,2})[b_{1+}[-(K^2+F)a_{(k-2)m2}+Fa_{(k-2)m1}]$$

$$+[-(4+F)b_{1+}+Fb_{2+}]a_{(k-2)m1}]$$

$$-(1-\delta_{k,-2})[b_{1-}[-(K^2+F)a_{(k+2)m2}+Fa_{(k+2)m1}]$$

$$+[-(4+F)b_{1-}+Fb_{2-}]a_{(k+2)m1}]\} = 0,$$

and

$$[(\omega-U_2k)(K^2+F)+k(\beta-FU_s)+irK^2]a_{k\ell 2} - (\omega-U_2k)Fa_{k\ell 1} = 0,$$

$$+2\pi\ell h_0/F\{\delta_{k,2}[b_{2+}[-(K_{\ell-}{}^2+F)a_{(k-2)\ell 1}+Fa_{(k-2)\ell 2}]$$

$$+[-(4+F)b_{2+}+F(b_{1+}+1)]a_{(k-2)\ell 2}]]$$

$$-\delta_{k,-2}[b_{2-}[-(K_{\ell+}{}^2+F)a_{(k+2)\ell 1}+Fa_{(k-2)\ell 2}]$$

$$+[-(4+F)b_{2-}+F(b_{1-}+1)]a_{(k+2)\ell 2}]]$$

$$+2\ell\pi h_0\sum_{\ell=1}^{\ell max}[\rho_{m\ell}\{$$

$$(1-\delta_{k,2})[b_{2+}[-(K^2+F)a_{(k-2)m1}+Fa_{(k-2)m2}]$$

$$+[-(4+F)b_{2+}+F(b_{1+}+1)]a_{(k-2)m2}]$$

$$-(1-\delta_{k,-2})[b_{2-}[-(K^2+F)a_{(k+2)m1}+Fa_{(k+2)m2}]$$

$$+[-(4+F)b_{2-}+F(b_{1-}+1)]a_{(k+2)m2}]\} = 0 \qquad (4.3)$$

where $\rho_{m\ell}$ is defined by

$$\cos \ell\pi y = \sum_{m=1}^{\infty} \rho_{m\ell} \sin m\pi y; \tag{4.4}$$

i.e.,

$$\rho_{m\ell} = \begin{cases} 2/\pi[1/(m+\ell)+1/(m-\ell)] & \text{if } m\pm\ell \text{ odd}, \\ 0 & \text{if } m\pm\ell \text{ even}, \end{cases} \tag{4.5}$$

$$\delta_{k,k'} = 1 \text{ if } k=k'; \text{ otherwise } \delta_{k,k'}=0, \tag{4.6}$$

and

$$K_{m\pm}^2 = (k\pm 2)^2+m^2\pi^2.$$

The matrix eigenvalue approach is taken, in which the state of the system is represented by Q and the dynamics of the system are represented in the form

$$Q_t + \underset{\sim}{A}\, Q = 0. \tag{4.7}$$

If we write $Q = \mathrm{Re}\{ q \exp(-i\omega t)\}$, then eq. (4.7) gives

$$(\underset{\sim}{A} - i\,\omega\, \underset{\sim}{I})\, q = 0. \tag{4.8}$$

Define potential vorticities

$$Q_{k\ell n} = -(K^2+F)a_{k\ell n} + F\, a_{k\ell(3-n)}, \tag{4.9}$$

for n=1,2. Then we can express the streamfunction amplitudes as

$$\begin{aligned} a_{k\ell 1} &= -[FQ_{k\ell 1}+(K^2+F)Q_{k\ell 1}]/K_F, \\ a_{k\ell 2} &= -[FQ_{k\ell 2}+(K^2+F)Q_{k\ell 2}]/K_F, \end{aligned} \tag{4.10}$$

where $K_F=K^2(K^2+2F)$. Equations (4.3) can be rewritten in terms of the $Q_{k\ell 1}$ and $Q_{k\ell 2}$:

$$\begin{aligned} &ir_1\ell^2\pi^2[F\,Q_{0\ell 2} + (\ell^2\pi^2+F)\,Q_{0\ell 1}]/K_F \\ &+ (h_0/F)2\pi\ell\{[Q_{-2\ell 1}b_{1+}-Q_{2\ell 1}b_{1-}] \\ &\qquad + [(4+F)b_{1+}-Fb_{2+}][FQ_{-2\ell 2}+(K^2+F)Q_{-2\ell 1}]/[2^2(2^2+2F)] \\ &\qquad + [(4+F)b_{1-}-Fb_{2-}][FQ_{2\ell 2}+(K^2+F)Q_{2\ell 1}]/[2^2(2^2+2F)]\} \\ &\qquad - \omega\, Q_{0\ell 1} = 0, \end{aligned}$$

$$\begin{aligned} &ir_2\ell^2\pi^2[F\,Q_{0\ell 1} + (\ell^2\pi^2+F)\,Q_{0\ell 1}]/K_F \\ &\quad + 2\ell\pi h_0/F\{[Q_{-2\ell 2}b_{2+}-Q_{2\ell 2}b_{2-}] \\ &\quad + [(4+F)b_{2+}-Fb_{1+}+F][FQ_{-2\ell 1}+(K^2+F)Q_{-2\ell 2}]/[2^2(2^2+2F)] \\ &\quad - [(4+F)b_{2-}-Fb_{1-}+F][FQ_{2\ell 1}+(K^2+F)Q_{2\ell 2}]/[2^2(2^2+2F)]\} \\ &\qquad\qquad -\omega\, Q_{0\ell 2} = 0, \end{aligned}$$

$$kU_1Q_{k\ell 1} - [k(\beta+FU_s+ir_1K^2][FQ_{k\ell 2}+(k^2+F)Q_{k\ell 1}]/K_F$$

$$+ 2\ell\pi(h_0/F)(\sum_{m=1}^{\ell max}\{\rho_{m\ell}(1-\delta_{k,2}) \; [\; Q_{(k+2)m1}b_{1-}$$

$$- [(4+F)b_{1+}-Fb_{2+}][FQ_{(k-2)m2}+(K^2+F)Q_{(k-2)m1}]/K_{Fm-}]$$

$$- \rho_{m\ell} \; (1-\delta_{k,-2}) \; [\; Q_{(k-2)m1}b_{1+}$$

$$- [(4+F)b_{1-}-Fb_{2-}][FQ_{(k+2)m2}+(K^2+F)Q_{(k+2)m1}]/K_{Fm+}]$$

$$+ \delta_{k,2} \; [Q_{0\ell 1}b_{1+} - [(4+F)b_{1+}-Fb_{2+}][FQ_{0\ell 2}+(K^2+F)Q_{0\ell 1}]/KFm-]$$

$$- \delta_{k,-2} \; [Q_{0\ell 1}b_{1-} - [(4+F)b_{1-}-Fb_{2-}][FQ_{0\ell 2}+(K^2+F)Q_{0\ell 1}]/KFm+]$$

$$-\omega \; Q_{k\ell 1} = 0,$$

and

$$kU_2Q_{k\ell 2} - [k(\beta-FU_s)+ir_2K^2] \; [FQ_{k\ell 1}+(K^2+F)Q_{k\ell 2}]/K_F$$

$$+ 2\ell\pi(h_0/F)(\sum_{m=1}\{\rho_{m\ell}(1-\delta_{k,2}) \; [\; Q_{(k+2)m2}b_{2-}$$

$$- [(4+F)b_{2+}-F(b_{1+}+1)][FQ_{(k-2)m1}+(K^2+F)Q_{(k-2)m2}]/K_{Fm-}]$$

$$- \rho_{m\ell} \; (1-\delta_{k,-2}) \; [\; Q_{(k-2)m2}b_{2+}$$

$$- [(4+F)b_{2-}-F(b_{1-}+1)][FQ_{(k+2)m1}+(K^2+F)Q_{(k+2)m2}]/K_{Fm+}]$$

$$+ \delta_{k,2} \; [Q_{0\ell 2}b_{2+} - [(4+F)b_{2+}-F(b_{1+}+1)][FQ_{0\ell 1}+(K^2+F)Q_{0\ell 2}]/KFm-]$$

$$- \delta_{k,-2} \; [Q_{0\ell 2}b_{1-} - [(4+F)b_{2-}-F(b_{1-}+1)][FQ_{0\ell 1}+(K^2+F)Q_{0\ell 2}]/KFm+]$$

$$-\omega \; Q_{k\ell 2} = 0, \qquad (4.11)$$

where

$$\ell_F = \ell^2\pi^2(\ell^2\pi^2+F),$$

$$K_{Fm\pm}=K_{m\pm}^2(K_{m\pm}^2+2F),$$

$$K_{2\ell}^2=2^2+\ell^2\pi^2,$$

$$K_{F2\ell}=K_{2\ell}^2(K_{2\ell}^2+2F). \qquad (4.12)$$

Each equation in (4.11), representing one row of the matrix in eq. (4.8), is used to compute the matrix coefficients, and the eigenvalues and eigenvectors associated with the matrix are found with standard eigenvalue solving mathematical subroutines.

The coupling in (4.11) is between the zonal wavenumber k and k±2k'. So the equations for odd k are decoupled from even k. For odd k, there is no coupling between a wavenumber pair (k,ℓ) and (k±2,ℓ), since $\rho_{m\ell} = 0$. For even k this is also true, except that (-2,ℓ), (0,ℓ) and (2,ℓ) are all coupled because $\rho_{m\ell}$ did not enter into these equations. Then, eqs. (4.11) can be written for four collections of wavenumbers, each consisting of wavenumber pairs that are coupled, and which are totally decoupled from wavenumbers present in other collections. We shall refer to these collections as set numbers 1,...,4. By convention, sets 1 and 2 will have even zonal wavenumbers and sets 3 and 4 have odd zonal wavenumbers. Set number 1 has (k,ℓ) = (0,1) as a member, and set number 3 has (k,ℓ) = (1,1) as a member. As an example, if the system of

equations is truncated at kmax = 6 and ℓmax = 4; i.e., $-6 \le k \le 6$ and $1 \le l \le 4$, we will define set numbers 1,..,4 as follows:

Set #1:

$(k,\ell) \in \{(-6,1),(-6,3),(-4,2),(-4,4),(-2,1),(-2,3),(0,1),$
$(0,3),(2,1),(2,3),(4,2),(4,4),(6,1),(6,3)\}$

Set #2:

$(k,\ell) \in \{(-6,2),(-6,4),(-4,1),(-4,3),(-2,2),(-2,4),(0,2),$
$(0,4),(2,2),(2,4),(4,1),(4,3),(6,2),(6,4)\}$

Set #3:

$(k,\ell) \in \{(-5,2),(-5,4),(-3,1),(-3,3),(-1,2),(-1,4),(1,1),$
$(1,3),(3,2),(3,4),(5,1),(5,3)\}$

Set #4:

$(k,\ell) \in \{(-5,1),(-5,3),(-3,2),(-3,4),(-1,1),(-1,3),(1,2),$
$(1,4),(3,1),(3,3),(5,2),(5,4)\}$.

4.2 Growth Rate:

The growth rate is decreased only slightly by the inclusion of topography for the parameter ranges of interest. For F=35, $r_1=r_2 = 2$, the growth rate is decreased on the order of .04 day^{-1} as the topography height h_0 is increased from 0 to 10. We can define a function $u(h_0;\omega_i)$ to be the shear U that yields a growth rate of ω_i for a topography height h_0. We find that u is approximately given by

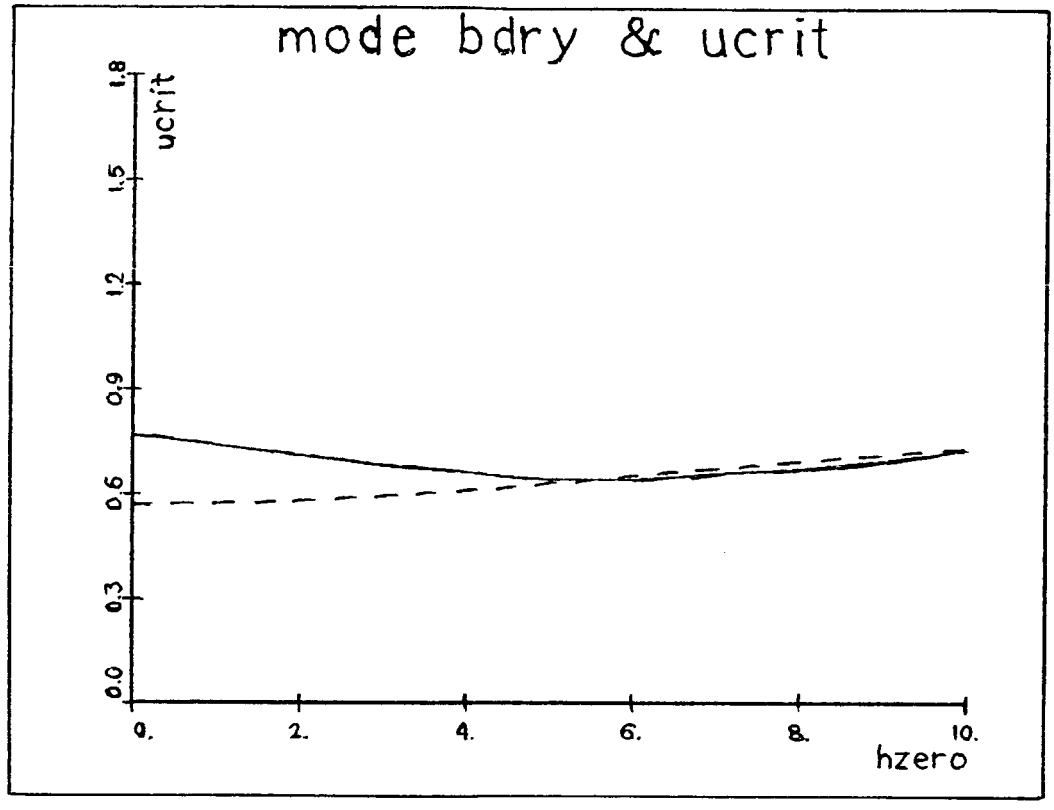

Figure 4.1 The transition from wavenumber 4 to wavenumber 5 as the dominant zonal wavenumber of the fastest-growing eigenmode (solid line), and the marginal curve (dashed line), as functions of the shear U_s and topography height h_0, for F = 35, U_2 = .15, β = 0, and $r_1 = r_2$ = 1.5. The dominant meridional wavenumber is ℓ = 1.

$$u(h_0,\omega_i) = u_0\ (1 + \alpha\ h_0^2), \qquad (4.13)$$

where α is approximately .002.

Of greater importance are structural changes introduced by the topography. Near the minimum critical shear, the asymptotic model showed long waves to be stabilized more than short waves (Fig. 3.6), and hence, for some parameter values the topography can give rise to an increased dominant wavenumber of the fastest growing mode. An increase in the zonal wavenumber as h_0 increases is suggested by Fig. 4.1 for $0<h_0<7$; and for $h_0>7$, the wavenumber decreases, but at this parameter setting, the wave is not unstable.

4.3. Streamfunction:

The relative amplitudes associated with the various wavenumbers for the most unstable eigenmode when F=35, $h_0 = 5$, and $r_1=r_2 = 2$, is shown in Fig. 4.2. The dominant wavenumber is $(k,\ell) = (5,1)$. The sidebands picked up by the asymptotic model are of wavenumbers 3 and 7. A wavenumber 1 effect that is not part of the asymptotic model solution is also present. In the lower layer, this wavenumber 1 component is larger than the wavenumber 3 component.

Time series of the streamfunction field for the above choice of parameters are shown in Fig. 4.3, where only half the zonal extent of the domain is shown. The streamfunction field

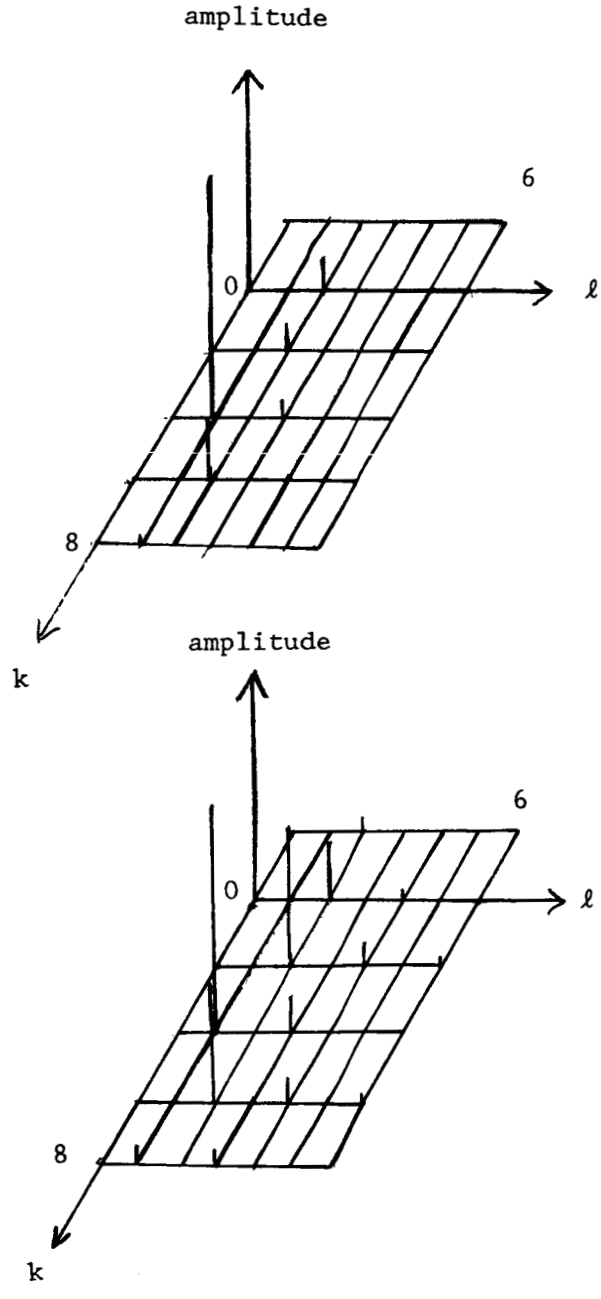

Figure 4.2 The relative amplitudes of various Fourier components making up the most unstable eigenmode, for F=35, U_2=.15, β=0, h_0 = 5, and r_1 = r_2 = 1.5.

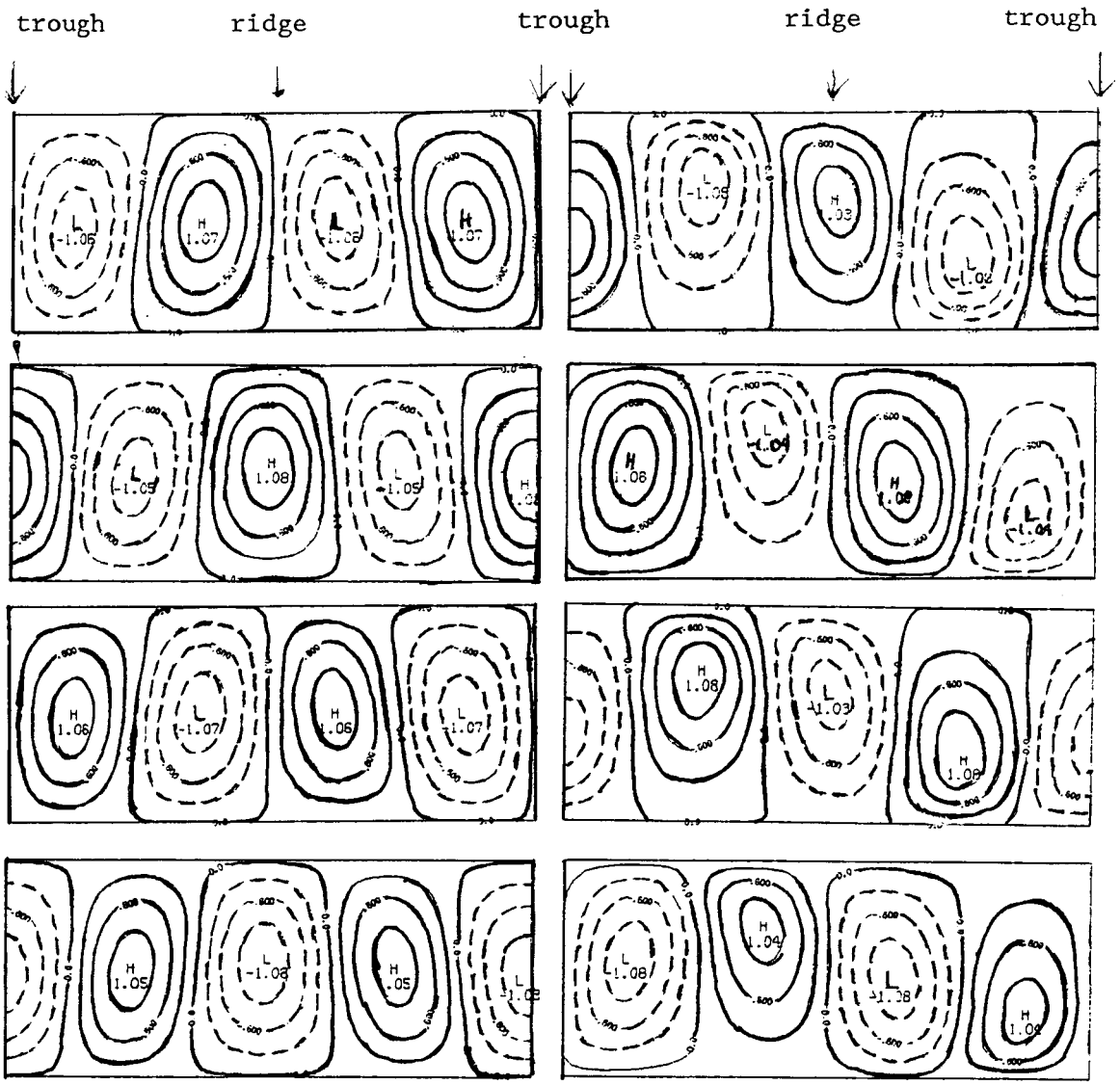

Figure 4.3 The streamfunction ϕ_n^t for layers n=1,2, computed for times $\omega_r t = 0, \pi/2, \pi$, and $3\pi/2$, using the numerical model, for U_2=.15, F=35, $h_0 = 5$, β=0, and $r_1 = r_2 = 1.5$. Only the half of the domain $-\pi/2 \leq x \leq \pi/2$ is shown. Topographic ridge and trough positions are shown at the top.

agrees very well with that obtained from the asymptotic model in Fig. 3.5.

4.4 Effects of Truncation:

First we consider the inviscid problem in which the Fourier expansion in eq. (4.1) is truncated to the zonal flow and the topography wavenumber. This is the simplest scenario in which we could address the question of whether a stationary wave might arise form the case of U_2 equal to zero. A nontrivial solution to eqs (4.3) can be found by setting the determinant of the matrix of coefficients of the $a_{k\ell n}$'s equal to zero. The result is the following biquadratic equation:

$$[\omega^2+b]^2 - c^2\omega^2 = 2\ \gamma\ [\omega^2 + b+ac], \tag{4.14}$$

where

$$a = -2\ U + \frac{2\ (\beta + FU)}{K^2 + F} = \frac{2\ (\beta-UK^2)}{K^2 + F}, \tag{4.15}$$

$$b = \frac{4\ (\beta - FU)\ (\beta - U\ K^2)}{K^2\ (\ K^2 + 2\ F)}, \tag{4.16}$$

$$c = -\ 2\ U + \frac{4\ \beta\ (K^2 + F)}{K^2\ (K^2 + 2F)}, \tag{4.17}$$

and

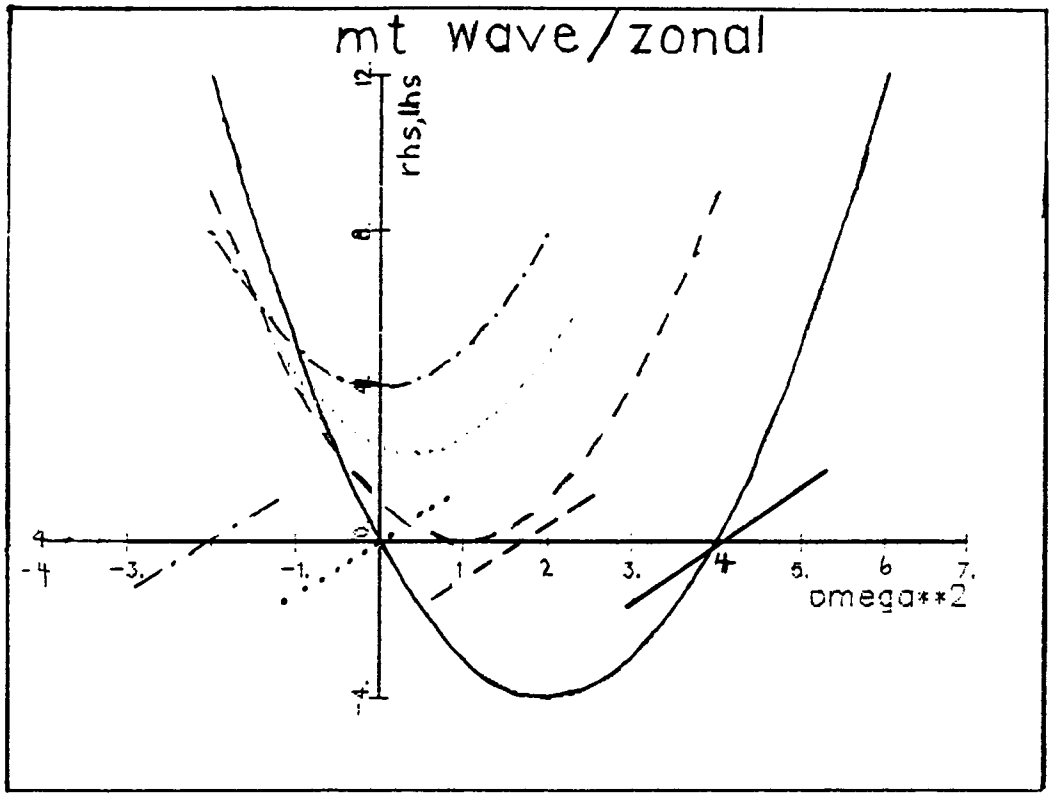

Figure 4.4 The right-hand side and the left-hand side of the dispersion relation, eq. (4.14). The curves shown are for F=0 (solid), F=7 (dashed), F=14 (dotted), and F=1000 (dot-dashed).

$$\gamma = \frac{4\, h_0^2\, (\ell^2\pi^2 + F)\,(K^2 + F)}{(\ell^2\pi^2 + 2F)\, K^2\, (K^2 + 2F)}. \qquad (4.18)$$

Although ω^2 is in general complex, the case of ω^2 real gives us some insight into the nature of the solution. The left-hand side of eq. (4.3) is a parabola centered at $(c^2/2\text{-}b, c^2(b\text{-}c^2/4))$ and the the right-hand side is a line of slope γ passing through the point $(-b\text{-}ac, 0)$. A solution is obtained whenever the two sides of eq. (4.3), shown in Fig. 4.4, are equal. If the line and parabola intersect, then there is a solution for real ω^2. If ω^2 is positive, then we have a **neutral** eigensolution. If ω^2 is negative, the solution will be **pure imaginary**; i.e., the perturbation is growing without an oscillatory behavior. If the line and parabola do not intersect, then the perturbation has a complex growth rate; i.e., it has a growing and an oscillatory behavior.

In Fig. 4.4, we see that for $F > 7$, ω^2 without topography is complex. The solution is a travelling baroclinic wave with $k = \pm 2$. If $F > 21$, then as γ increases, implying increasing h_0, there are two critical values of γ, namely $\gamma_{c1} < \gamma_{c2}$ such that for $\gamma_{c1} < \gamma < \gamma_{c2}$ there are four neutral solutions, and for $\gamma > \gamma_{c2}$ there are two neutral solutions and two non-oscillatory growing solutions. For $7 < F < 21$, γ_{c2} does not exist. For F less than 7, topography destabilizes neutral modes. The remaining discussion is for $F > 21$.

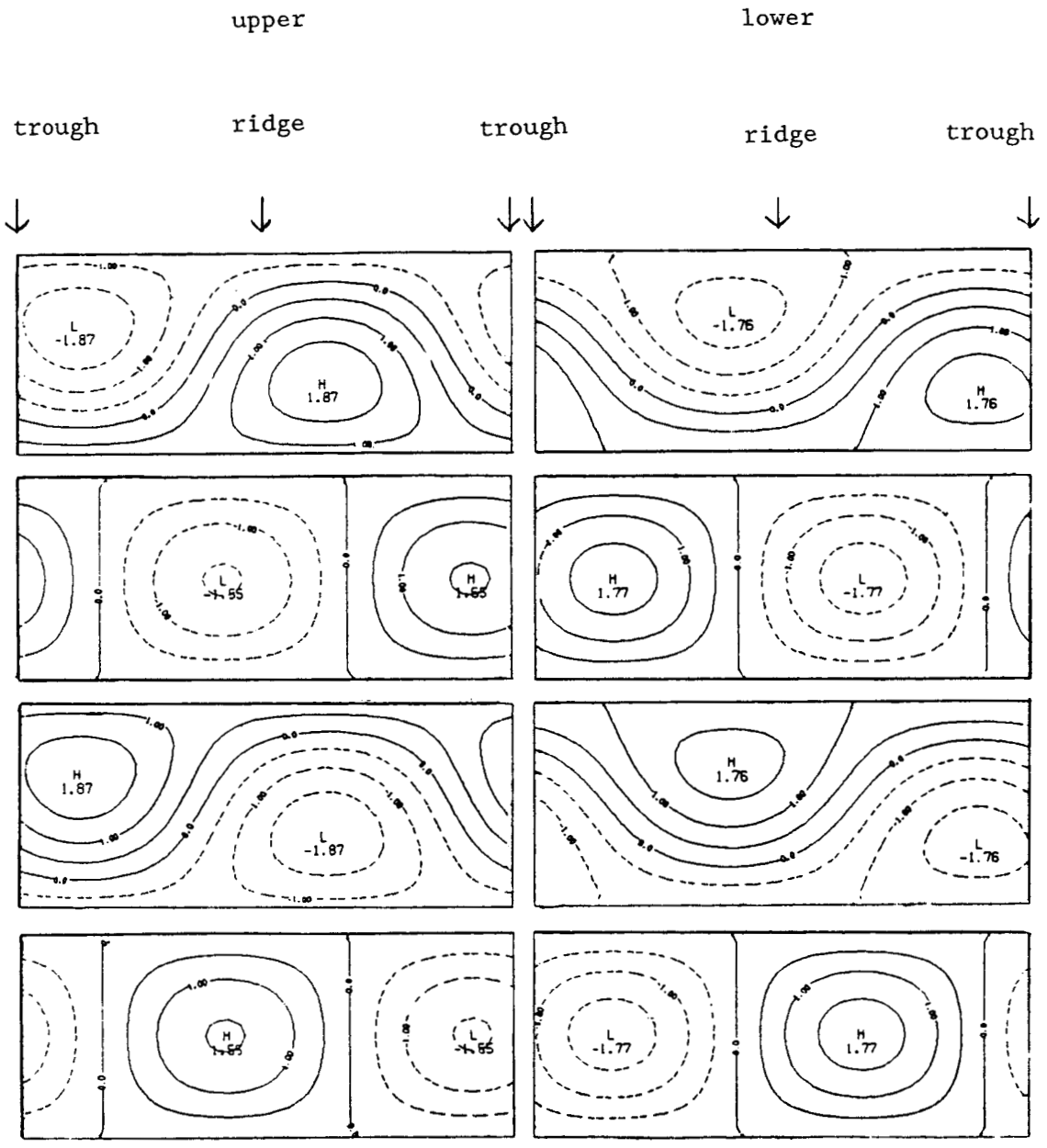

Figure 4.5 As in Fig. 4.3, except for the severely truncated problem (wavenumbers k = 2, 0, and -2), with $r_1 = r_2 = 0$, $U_2 = 0$, and $h_0 = 2$.

The streamfunction pattern for the case of $\gamma < \gamma_{c1}$, shown in Fig. 4.5, is a pattern of highs and lows travelling on a meandering path, as was the case of a baroclinic wave modified by topography presented in Figs. 3.5 and 4.3. In addition, Fig. 4.5 reveals an index cycle vacillation, due to the presence of a zonal flow in the perturbation. At time $\omega_r t$ equal to 0 (π), the flow has a high (low) zonal index.

The case of $\gamma > \gamma_{c2}$, shown in Fig. 4.6, is a stationary disturbance, with a ridge centered over (shortly upstream from) the topographic ridge in the lower (upper) layer.

The above discussion concerns a severe truncation. Except for a restricted region in parameter space, viz. for relatively small F, the 2,0,-2 truncation does not yield the most unstable mode. Hence this mode may not be physically relevant, unless it dominates in a finite amplitude problem, as some less unstable modes do in Hart (1981) and Nathan (1985). The numerical eigenvalue problem was run for the viscous case to determine if this mode arises at the parameter setting we have considered. The critical topography height at which the topographic instability for F=35 is equal to approximately 6 for the inviscid case, and increases for viscous cases. Hence it is more reasonable to assume that the stationary wave arises due to a nonzero lower layer basic state velocity, and not due to a topographic instability with a zero basic state lower velocity.

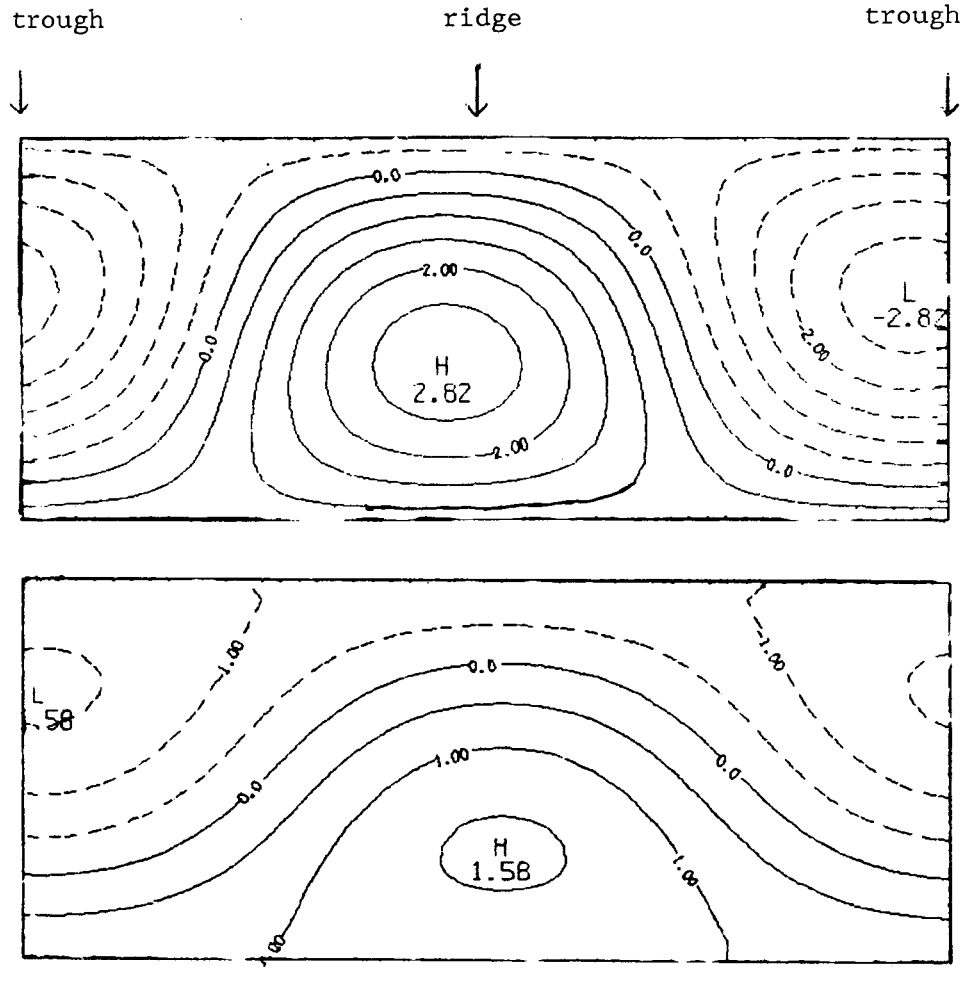

Figure 4.6 As in Fig. 4.5, except for $h_0 = 6$, and only at time $t = 0$.

Table 4.1 : Growth rates as a function of wavenumber for some selected topography heights, for two truncation levels.

Truncation 1: $k_{max} = 12$, $\ell_{max} = 6$:

h_0:		0	5	6
Dominant k:	1	.427	.216	.172
	2	.82	0.0	.314(ω_r=0)
	3	1.14	.952	.896
	4	1.36	1.22	1.18
	5	1.45	1.36	1.32
	6	1.37	1.33	1.31
	7	1.03	1.05	1.05
	8	0.0	.29	.37

Truncation 2: kmax = ℓ_{max}=2:

h_0:		0	5	6
Dominant k:	2	.82	0.0	.334(ω_r=0)

In table 4.1 is shown a plot of growth rate as a function of wavenumber for the inviscid dase with $U_2 = 0$, for $h_0 = 0$, 5, and 6, for $k_{max} = 12$, $\ell_{max} = 6$, for $h_0 = 0$, 5, and 6. Stabilization due to the topography occurred for all wavenumbers, except near the short-wave cutoff and also with the notable exception of wavenumber 2, which exhibits the topographic instability for $h_0 \geq 6$. Hence the severely truncated scenario described above is present when the severe truncation is relaxed.

The effect of truncation on the most unstable eigenvalue ω for $F = 35$ and $r_1 = r_2 = 1.5$ were determined for $k_{max} = \ell_{max}$ up to 10. Results for $h_0 = 5$ are shown in Table 4.2. For fixed $k_{max} \geq 8$, it appears that $\ell_{max} = 6$ is sufficient meridional resolution to determine the eigenvalue accurately. Also $k_{max} = 8$ appears to be sufficient zonal resolution. The appropriate value for k_{max}, and to a lesser extent ℓ_{max} increase with increasing F, since the dominant wavenumber is a function of F as given in Chapter 3. The number of wavenumbers required in these results is not nearly as great as in Niehaus (1980), who studied wave stability. One might suspect that the coupling of zonal harmonics in wave-stability problems would be stronger than in this problem, where imposed waves do not occur at leading order.

The change in growth rate, $\Delta\omega_i$, and frequency, $\Delta\omega_r$, introduced by topography were computed for the numerical model

Table 4.2: The nondimensional growth rate as a function of the modal truncation, for $h_0 = 5$, $F = 35$, $\beta = 0$, $U_2 = .15$, and $r_1 = r_2 = 1.5$.

k_{max}	ℓ_{max}	Growth rate
4	2	.276
4	≥4	.273
6	2,4,6	.303
6	≥8	.297
8	2	.273
8	≥4	.270
10	2	.273
10	≥4	.270

and compared with the asymptotic model. The percent discrepancy ϵ_n was computed using the following definition:

$$\epsilon_{ni} = \frac{[(\Delta\omega_i)_n - (\Delta\omega_i)_a]}{[(\Delta\omega_i)_a{}^2+(\Delta\omega_r)_a{}^2]^{1/2}} \cdot 100\%,$$

$$\epsilon_{nr} = \frac{[(\Delta\omega_r)_n - (\Delta\omega_r)_a]}{[(\Delta\omega_i)_a{}^2+(\Delta\omega_r)_a{}^2]^{1/2}} \cdot 100\%,$$

where

$$(\Delta\omega_r)_a = \omega_r\Big|_{h_0} - \omega_r\Big|_{\text{no topo.}},$$

$$(\Delta\omega_i)_a = \omega_i\Big|_{h_0} - \omega_i\Big|_{\text{no topo.}},$$

for the asymptotic model, and

$$(\Delta\omega_r)_n = \omega_r\Big|_{h_0} - \omega_r\Big|_{\text{no topo.}},$$

$$(\Delta\omega_i)_n = \omega_i\Big|_{h_0} - \omega_i\Big|_{\text{no topo.}},$$

for the numerical model with $k_{max} = 10$ and $\ell_{max} = n$, and these results are plotted in Fig 4.7. Most of these results are

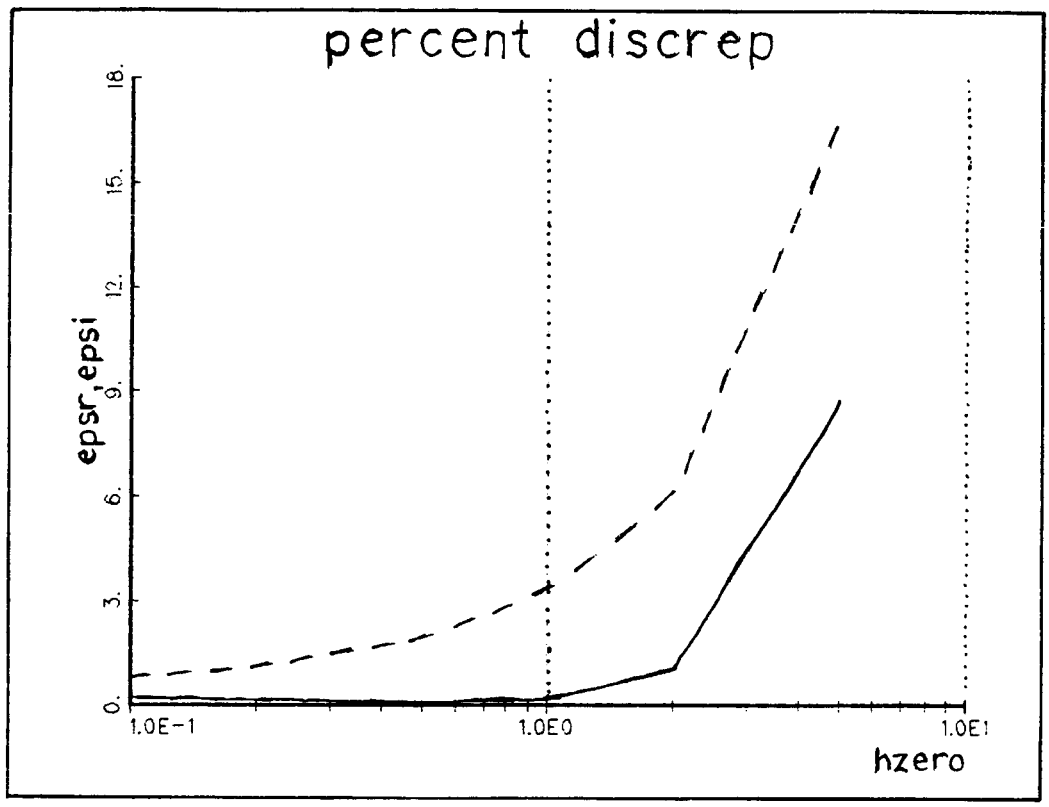

Figure 4.7 The percent discrepancy ϵ_{6r} (solid) and ϵ_{6i} (dashed), between the topographic effects on the frequency and growth, respectively, for β=0, F=35, and $r_1 = r_2 = 1.5$, for various values of h_0, where $k_{max} = 10$.

almost identical to those obtained with $k_{max} = 8$. The residual in the discrepancy as k_{max} and ℓ_{max} go to infinity measures the error inherent in the small h_0 approximation used in the asymptotic model.

For the point in parameter space given in Fig. 4.7, the two models disagree much more in the growth rates $\Delta\omega_i$ than in the frequency change $\Delta\omega_r$. Also we find the absolute value of $\Delta\omega_r$ to be smaller than the absolute value $\Delta\omega_i$. This is not true when one looks at some other points in parameter space; e.g., F=20, shown in Table 4.3. In all the cases run, for h_0 less than or equal to 5, we find the frequency to be increased by the presence of the topography.

Since $\psi_n^{(3)}$ from the asymptotic model does not project onto the wavenumber of the leading order disturbance, one would expect the models to agree to order $(h_0/F)^4$. The errors appear to be of order $(h_0/F)^3$, due primarily to the fact that coupling terms due to the topography in the matrix in equation (4.7) include a factor of $2\pi\ell$: the factor of 2 from the x-derivative of the topography height, and $\pi\ell$ from the y-derivative of the wave streamfunction. The largest discrepancies occur when F is large, which means h_0 is large when h_0/F is fixed. The ratios of some terms that do not depend on F; for example the comparison between the advection and topography terms in the original formulation, might become important.

Table 4.3: The percent discrepancies ϵ_r and ϵ_i for various values of F/r_2 and F, with h_0/F equal to .1, $U_1 = 1$, $U_2 = .15$.

F	F/r_2	ϵ_r	ϵ_i
20	20	6.75	4.68
40	20	3.1	11.1
60	20	.05	15.4
20	200	8.92	6.09
40	200	3.57	17.08
60	200	3.89	26.67

4.5 Phase Speed:

The dominant wavenumber, i.e., the wavenumber k of the leading order solution, can be used to define a phase speed; i.e.,

$$c_r = \omega_r/k$$

The phase velocity was found to be affected only slightly by the topography, increasing on the order of a few per cent as the topography is varied from 0 to 5.

V. CONCLUSIONS

The observations of some features of the flow field in the atmosphere and in the annulus experiments of LKP have been compared with results of a linear theory. Notably, the observations indicate a tendency for a ridge to exist upstream of the topography due to the presence of a stationary wave forced by the interaction of the lower layer zonal flow and the topography.

The transient disturbance involves a coupling of various zonal wavenumbers by the topography and the parameterized stationary waves. When parameters are chosen appropriately for the atmosphere and the annulus, the fastest-growing eigenmode is a baroclinic wave, modulated by the topography, causing the eastward-travelling cyclones and anticyclones to meander along a sinusoidal path that is fixed in time. The cyclone and anticyclone centers reach their minimum latitude at about one-third of a topographic wavelength downstream from the ridge, and the maximum latitude one-sixth wavelength upstream. The phase of this path relative to the topography is in qualitative agreement with the observational results of Blackmon, et al. (1977) shown in Figure (1.1b).

The form of the transient disturbance is essentially the

same for the cases of zero and nonzero lower layer basic state velocity. Hence the meandering wave is present for the case of no lower-layer velocity, but in this case the forced stationary wave is absent.

The transient disturbance alone cannot capture much longitude dependence of the strength of cyclones and anticyclones. However, the sum of the stationary and transient disturbances yields a flow pattern characterized by a tendency toward high pressure shortly upstream of the topographic ridge and low pressure shortly upstream of the topographic trough, which is in qualitative agreement with the observed results.

The eigenvalues obtained in this study show the topography to stabilize baroclinic waves except near the short-wave cutoff and to shift the maximum instability to shorter wavelengths for small topography. The eigenvalue changes are small, of order $(h_0/F)^2$.

The asymptotic and numerical model results agree to order $(h_0/F)^3$. Hence there is good agreement for moderately large h_0, since F is large enough to keep h_0/F small. Physically, large F implies that the length scale of the most unstable wave is much shorter that the wavenumber 2 topography; hence the magnitude of topographically-induced vertical motions on a baroclinic wave is smaller than for an equivalent problem with small F. One might suspect that the agreement should be of order $(h_0/F)^4$, based on the asymptotic model formulation. Some

further check on the magnitudes of the various terms might be required to verify this.

If one truncates the Fourier expansion of the perturbation in the numerical model to include only the zonally-averaged flow and the zonal wavenumber of the topography, the inviscid dispersion relation reduces to a biquadratic which yields a topographically-modified baroclinic instability for small topography and a topographic instability, in which waves grow in situ, for large topography. For intermediate values of h_0, the waves are neutrally stable. The eigenmodes obtained from this truncation were not the most unstable for the values of F relevant to the planetary-scale atmosphere. It remains to be seen if they might be important in a nonlinear model.

This study can be extended in several ways. The stationary wave problem was arbitrarily simplified, in order to facilitate the analysis. There is a latitude-dependence of the stationary wave that was removed by parameterization. Inclusion of this additional y-structure would probably destroy the antisymmetry that leads to the meandering of the time-dependent solutions and that leads to an expectation of the vanishing of the phase oscillation of the wavenumber 2 component in the middle of the channel, a feature which is not observed in the experimental data. The results of LKP also suggest the possible presence of stationary wavenumber 4 and wavenumber 6 components. The solu-

tion of the time-independent equations should be extended to include these.

It would be interesting to investigate the robustness of these conclusions in a nonlinear study. One question is whether one must specify the lower-layer velocity in the basic state. A nonlinear model is capable of generating a zonal flow correction. Nonlinear interactions could lead to the excitation of a topographic instability. It is desirable to see what sort of modes survive, their time evolution, and the types of final states which are present in various regions of parameter space.

REFERENCES

Blackmon, M.L., 1976: A climatological spectral study of the 500 mb geopotential of the Northern Hemisphere. J. Atmos. Sci., 33, 2285-2291.

Blackmon, M.L., J.M. Wallace, N.-C. Lau, and S.L. Mullen, 1977: An observational study of the Northern Hemisphere Wintertime Circulation. J. Atmos. Sci., 34, 1040-1053.

Charney, J.G. and J.G. DeVore, 1979: Multiple flow equilibria in the atmosphere and blocking. J. Atmos. Sci., 36, 1205-1216.

Charney, J.G. and D.M. Straus, 1980: Form-drag instability, multiple equilibria, and propagating planetary waves in baroclinic, orographically forced planetary wave systems. J. Atmos. Sci., 37, 1157-1176.

De Szoeke, R.A., 1975: Some effects of bottom topography on baroclinic instability. J. Marine Res., 33, 93-122.

De Szoeke, R.A., 1983: Baroclinic instability over wavy topography. J. Fluid Mech., 130 279-298.

Durney, B.R., 1977: The influence of mesoscale topography on the stability and growth rates of a two-layer model of the open ocean. Geo. Astroph. Fluid Dyn., 9, 115-128.

Fredericksen, J.S., 1979: The effects of long planetary waves on the regions of cyclogenesis: Linear theory. J. Atmos. Sci., 36, 195-204.

Gates, W.L., 1961: Static stability measures in the atmosphere. J. Met., 18, 526-533.

Hart, J.E., 1979: Barotropic quasi-geostrophic flow over anisotropic mountains. J. Atmos. Sci., 36, 1736-1746.

Hart, J.E., 1981: Wavenumber selection in nonlinear baroclinic instability. J. Atmos. Sci., 38, 400-408.

Li, Q.G., R. Kung, and R.L. Pfeffer, 1986: An experimental study of baroclinic flows with and without two-wave bottom topography. (In press).

Nathan, T.R., 1985: Interactions between unstable baroclinic and resonant, topographic waves in a two-layer model of the atmosphere. Ph.D. dissertation, State Univ. of N.Y. at Albany, 106pp.

Niehaus, M.C.W., 1980: Instability of non-zonal baroclinic flows. J. Atmos. Sci., 38, 974-987.

Pedlosky, J., 1979: Geophysical Fluid Dynamics, Springer-Verlag, 624 pp.

Pedlosky, J., 1981: Resonant topographic waves in barotropic and baroclinic flows. J. Atmos. Sci., 38, 2626-2641.

Peixoto, J.P., B. Saltzman and S. Teweles, 1964: Harmonic analysis of the topography along parallels of the earth. J. Geophys. Res., 69, 1501-1505.

Tibaldi,S. and A. Buzzi, 1983: Effect of orography on Mediterranean lee cyclogenesis and its relationship to European blocking. Tellus, 35A, 269-286.

APPENDIX A:

ORTHOGONALITY CONDITION FOR ASYMPTOTIC MODEL

The orthogonality condition will be presented for the case of $U_2 = 0$ and $U_1 = U$, but the result for general U_2, to which the method readily extends, will also be stated. The leading order problem from eq. (3.1) can be written in terms of the lower-layer streamfunction; i.e. in the following form:

$$\mathcal{L}^{(0)}\ \psi_2^{(0)} = 0, \tag{A.1}$$

with boundary conditions

$$\psi_2^{(0)} = L_2\psi_2^{(0)} = 0 \qquad \text{at } y = 0,1. \tag{A.2}$$

The solution to this problem was given in eqs. (3.4)-(3.5), and for $U_2 = 0$, it is given by

$$\psi^{(0)} = \exp(ikx)\sin \ell\pi y, \tag{A.3}$$

$$\omega^{(0)} = k/2\{c_+ - i\alpha' \pm [c_-^2 - 2i\alpha c_+ - \alpha'^2 + 4\alpha]^{1/2}\}, \tag{A.4}$$

where c_+, c_-, α', and α were defined in eqs (3.6).

The order h_0/F problem is given by representing eqs.

(3.10-3.11) in the form

$$\mathcal{L}^{(1)}\psi_2^{(0)} + \mathcal{L}^{(0)}\psi_2^{(1)} + 8L_1^{(0)}[\sin 2x\ \psi_{2y}^{(0)}] = 0 \qquad (A.5)$$

with boundary conditions

$$\psi_2^{(1)} = L_2^{(0)}\psi_2^{(1)} + L_2^{(1)}\psi_2^{(1)} + 8L_1^{(0)}[\sin 2x\ \psi_{2y}^{(0)}] = 0 \qquad (A.6)$$

In order to find $\omega^{(1)}$, we apply the solvability condition by multiplying (A.5) by the adjoint of (A.3) and integrating over the domain:

$$\int_0^1\int_0^{2\pi} (\psi_2^{(0)+})^*\mathcal{L}^{(1)}\psi_2^{(0)}\,dx\,dy + \int_0^1\int_0^{2\pi} (\psi_{2(0)+})^*\mathcal{L}^{(0)}\psi_2^{(1)}\,dx\,dy$$

$$4\int_0^1\int_0^{2\pi} (\psi_2^{(0)+})^*L_1^{(0)}[\sin 2x\psi_{2y}^{(0)}]\,dx\,dy = 0. \qquad (A.7)$$

where the superscript + represents the adjoint.

The adjoint problem for $\psi_2^{(0)}$ yields

$$\mathcal{L}^{(0)+}\psi_2^{(0)+} = 0, \qquad (A.8)$$

where $\psi_2^{(0)+} = \psi_2^{(0)} = \exp(ikx)\sin(\ell\pi y)$ and $\mathcal{L}^{(0)+}$ is the same as $\mathcal{L}^{(0)}$ except that the complex conjugate of $\omega^{(0)}$, denoted $\omega^{(0)*}$ is used in place of $\omega^{(0)}$.

The third term is zero since

$$L_1^{(0)}[\sin 2x\ \psi^{(0)}_y] \approx (\ )\exp(i(k+2)x) + (\ )\exp(i(k-2)x)$$

and therefore the product of this and exp(-ikx) integrates over x to zero. The first term in Eq. (A.7) will be written

$$\int_0^1 \int_0^{2\pi} (\psi_2^{(0)+})^* \mathcal{L}^{(1)} \psi_2^{(0)}\ dx\ dy = \omega^{(1)} I \qquad (A.10)$$

The second term in Eq. (A.7) is evaluated using a Lagrange identity; i.e.,

$$\int_0^1 \int_0^{2\pi} (\psi_2^{(0)+})^* \mathcal{L}^{(0)} \psi_2^{(1)} dx\ dy - \int_0^1 \int_0^{2\pi} (\psi_2^{(1)})^* (\mathcal{L}^{(0)+} \psi_2^{(0)+})\ dx$$

$$= \int_0^{2\pi} [-i\omega^{(0)} - U\partial_x]\ [-i\omega^{(0)}]\ [(\psi_2^{(0)}{}_y)^* (-\psi_2^{(1)}{}_{yy})]\Big|_{y=0}^{y=1} dx$$

(plus other terms which are zero when the b.c. are applied)

(A.11)

But the remaining boundary term integrates to zero when $L_2^{(0)}\psi^{(1)}$ is expressed in terms of $\psi^{(0)}$ using the boundary condition

$$L_2^{(0)}\psi_2^{(1)} = -4 \sin 2x\ \psi_2^{(0)}{}_y$$

and substituted into the right-hand side of (A.11).

Also the second term on the left-hand side of (A.11) is zero, leaving

$$\omega^{(1)}\ I = 0 \qquad (A.12)$$

In general, I is nonzero, implying $\omega^{(1)} = 0$. This implies also that $\mathcal{L}^{(1)} = 0$, and then (3.10-3.11) become a forced differential equation for $\psi_2{}^{(1)}$ in terms of $\psi_2{}^{(0)}$:

$$\mathcal{L}^{(0)}\psi_2{}^{(1)} = -8L_1{}^{(0)}[\sin 2x\ \psi_2{}^{(0)}{}_y] \tag{A.13}$$

The solution $\psi_2{}^{(1)}$ has the form

$$\psi_2{}^{(1)} = g_{2+}(y)\exp(i(k+2)x) + g_{2-}(y)\exp(i(k-2)x) \tag{A.14}$$

The $O(h_0/F)^2$ problem is written

$$\mathcal{L}^{(2)}\psi_2{}^{(0)} + \mathcal{L}^{(0)}\psi_2{}^{(2)} + 4L_1{}^{(0)}[\sin 2x\ \psi_2{}^{(1)}{}_y] = 0 \tag{A.15}$$

with boundary conditions

$$\psi_2{}^{(1)} = L_2{}^{(0)}\psi_2{}^{(1)} + L_2{}^{(1)}\psi_2{}^{(1)} + 4L_1{}^{(1)}[\sin 2x\ \psi_2{}^{(0)}{}_y]=0 \tag{A.16}$$

At $O(h_0/F)^2$ the orthogonality condition on (A.15) yields

$$\int_0^1\int_0^{2\pi} (\psi_2{}^{(0)+})^*\mathcal{L}^{(2)}\psi_2{}^{(0)}\ dx\ dy + \int_0^1\int_0^{2\pi} (\psi_2{}^{(0)+})^*\mathcal{L}^{(0)}\ dx\ dy =$$

$$-4\int_0^1\int_0^{2\pi} (\psi_2{}^{(0)+})^*L_1{}^{(0)}(\sin 2x\psi_2{}^{(1)}{}_y)\ dx\ dy. \tag{A.17}$$

yielding

$$\omega^{(2)}I = I' + 4\pi^2 lF(\omega^{(0)}-Uk+ir_1)[\cos \ell\pi y\ (g_{2-y}-g_{2+y})]\Big|_{y=0}^{y=1}, \tag{A.18}$$

where the integral I is given by

$$\omega^{(2)}\ I = \int_0^1 \int_0^{2\pi} \psi_2{}^{(0)*} \mathcal{L}_2 \psi_2{}^{(0)}\ dx\ dy \tag{A.19}$$

$$= \pi\ \mu_{k\ell}$$

where

$$\mu_{k\ell} = -(K^2+F)[\omega^{(0)}(K^2+F)+2\beta k+(r_1+r_2)iK^2] + F^2(2\omega^{(0)}-Uk) \tag{A.20}$$

The integral I' is given by

$$I' = 4\pi^2 \ell F\{a_{2+}\xi(\lambda_{++})-a_{2-}\xi(\lambda_{-+})+a_{4+}\xi(\lambda_{+-})-a_{4-}\xi(\lambda_{--})$$
$$- 1/2(a_{5+}-a_{5-})[\mu'+\ell^2\pi^2(\omega^{(0)}-Uk+ir_1)]\}, \tag{A.21}$$

where

$$\mu' = (\omega^{(0)}-Uk)(k^2+F) + k(\beta+FU) + r_1 ik^2,$$

and when ℓ is even,

$$\xi(\lambda) = 2\lambda[\mu'+\lambda^2(\omega^{(0)}-Uk+ir_1)](\cos(\lambda/2))/(\ell^2\pi^2-\lambda^2),$$

and when ℓ is odd,

$$\xi(\lambda) = -2\lambda[\mu'+\lambda^2(\omega^{(0)}-Uk+ir_1)](\sin(\lambda/2))/(\ell^2\pi^2-\lambda^2).$$

For general U_2, equation (A.18) becomes

$$I = I' + I'', \tag{A.22}$$

where I' and I'' are given by

$$\begin{aligned} I' = 4\pi^2 \ell \{ & (\omega^{(0)} - U_1 k + i r_1)[b_{2-} I_{2,4+} - b_{2+} I_{2,4-} + B_{2-} I_{2,2+} \\ & - B_{2+} I_{2,2-} + b_{2-} F I_{1,2+} - b_{2+} F I_{1,2-}] \\ & - (\omega^{(0)} - U_2 k) F [b_{1-} I_{1,2+} - b_{1+} I_{1,2-} + B_{1-} I_{1,0+} - B_{1+} I_{1,0-} \\ & + b_{1-} F I_{2,0+} - b_{1-} F I_{2,0-}] \\ & - \mu' [b_{2-} I_{2,2+} - b_{2+} I_{2,2-} + B_{2-} I_{2,0+} - B_{2+} I_{2,0-} \\ & + b_{2-} F I_{1,0+} - b_{2+} F I_{1,0-}] \}, \end{aligned} \tag{A.23}$$

and

$$\begin{aligned} I'' = 4\pi^2 \ell (\omega^{(0)} - U_1 k + r_1 i) \cdot (& \left[b_{2-} \frac{d^2}{dy^2} + B_{2-} \right] g_{2+y} - \left[b_{2+} \frac{d^2}{dy^2} + B_{2+} \right] g_{2-y} \\ & + b_{2-} F g_{1+y} - b_{2+} F g_{1-y}) \cos \ell \pi y \Big|_{y=0}^{y=1} \end{aligned} \tag{A.24}$$

and where

$$I_{n,m\pm} = \int_0^1 \sin \ell \pi y \, \frac{d^{m+1}}{dy^{m+1}} g_{n\pm}(y) \, dy,$$

$$B_{1\pm} = -b_{1\mp}[(k\pm 2)^2 - 4] + b_{2\mp} F,$$

$$B_{2\pm} = -b_{2\mp}[(k\pm 2)^2 - 4] + (b_{1\mp} + 1) F. \tag{A.25}$$

APPENDIX B:

CALCULATION OF MERIDIONAL STRUCTURE COEFFICIENTS

The functions $g_{2\pm}$ are given in eqs. (3.17) and are repeated here:

$$g_{2+} = a_{1+} \cos(\lambda_{++}(y-1/2)) + a_{2+} \sin(\lambda_{++}(y-1/2) + a_{3+} \cos(\lambda_{+-}(y-1/2)) + a_{4+} \sin(\lambda_{+-}(y-1/2) + a_{5+}\cos \ell\pi y \tag{B.1}$$

$$g_{2-} = a_{1-} \cos(\lambda_{-+}(y-1/2)) + a_{2-} \sin(\lambda_{-+}(y-1/2)) + a_{3-} \cos(\lambda_{--}(y-1/2)) + a_{4-} \sin(\lambda_{--}(y-1/2)) + a_{5-}\cos \ell\pi y \tag{B.2}$$

First the coefficients $a_{5\pm}$ are found by the method of undetermined coefficients; i.e., we write a particular solution of eq. (3.14) in the form

$$g_p = a_{5\pm} \cos \ell\pi y, \tag{B.3}$$

resulting in

$$a_{5\pm} = \alpha_{3\pm} / [\ell^4\pi^4 - \alpha_{1\pm}\ell^2\pi^2 + \alpha_{2\pm}]. \tag{B.4}$$

These are substituted into the boundary conditions (3.15) to obtain, in the case of g_{2+},

$$a_{1+}\cos(\lambda_{++}/2) - a_{2+}\sin(\lambda_{++}/2)$$
$$- a_{3+}\cos(\lambda_{+-}/2) - a_{4+}\sin(\lambda_{+-}/2) + a_{5+} = 0, \tag{B.5}$$

$$a_{1+}\cos(\lambda_{++}/2) + a_{2+}\sin(\lambda_{++}/2)$$
$$- a_{3+}\cos(\lambda_{+-}/2) + a_{4+}\sin(\lambda_{+-}/2) + (-1)^{\ell}a_{5+} = 0, \tag{B.6}$$

$$a_{1+}(-\lambda_{++}+\alpha_4)\cos(\lambda_{++}/2) - a_{2+}(-\lambda_{++}+\alpha_4)\sin(\lambda_{++}/2)$$
$$- a_{3+}(-\lambda_{+-}+\alpha_4)\cos(\lambda_{+-}/2) - a_{4+}(-\lambda_{+-}+\alpha_4)\sin(\lambda_{+-}/2)$$
$$+ (-\ell^2\pi^2+\alpha_4)a_{5+} = \alpha_5, \tag{B.7}$$

$$a_{1+}(-\lambda_{++}+\alpha_4)\cos(\lambda_{++}/2) + a_{2+}(-\lambda_{++}+\alpha_4)\sin(\lambda_{++}/2)$$
$$- a_{3+}(-\lambda_{+-}+\alpha_4)\cos(\lambda_{+-}/2) + a_{4+}(-\lambda_{+-}+\alpha_4)\sin(\lambda_{+-}/2)$$
$$+ (-1)^{\ell}(-\ell^2\pi^2+\alpha_4)a_{5+} = (-1)^{\ell}\alpha_5. \tag{B.8}$$

If ℓ is odd, the sum (B.5)+(B.6) and the sum (B.7)+(B.8) yield only the trivial solution for a_{1+} and a_{3+}. Then eqs. (B.5) and (B.7) are solved simultaneously to yield

C.2

$$a_{2+}\,(\lambda_{++}^2-\lambda_{+-}^2)\,\sin(\lambda_{++}/2) = a_{5+}(\ell^2\pi^2-\lambda_{+-}^2)+\alpha_{5+},$$

$$a_{4+}\,(\lambda_{++}^2-\lambda_{+-}^2)\,\sin(\lambda_{+-}/2) = a_{5+}(\lambda_{++}^2-\ell^2\pi^2)-\alpha_{5+}.$$

If ℓ is even, the difference (B.5)-(B.6) and the difference (B.7)-(B.8) yield only the trivial solution for a_{2+} and a_{4+}. Then eqs. (B.5) and (B.7) are solved simultaneously to yield

$$a_{1+}\,(\lambda_{++}^2-\lambda_{+-}^2)\,\cos(\lambda_{++}/2) = a_{5+}(\lambda_{+-}^2-\ell^2\pi^2)-\alpha_{5+},$$

$$a_{3+}\,(\lambda_{++}^2-\lambda_{+-}^2)\,\cos(\lambda_{+-}/2) = a_{5+}(\ell^2\pi^2-\lambda_{++}^2)+\alpha_{5+}.$$

1. REPORT NO.	2. GOVERNMENT ACCESSION NO.	3. RECIPIENT'S CATALOG NO.
NASA CR-4057		

4. TITLE AND SUBTITLE	5. REPORT DATE
Linear Baroclinic Instability in the Presence of Large Scale Topography	MARCH 1987
	6. PERFORMING ORGANIZATION CODE

7. AUTHOR(S)	8. PERFORMING ORGANIZATION REPORT #
Nathaniel Dunton Reynolds	

9. PERFORMING ORGANIZATION NAME AND ADDRESS	10. WORK UNIT NO.
Universities Space Research Association 139 McMurtrie Lane Huntsville, AL 35814	M-553
	11. CONTRACT OR GRANT NO. NAS8-36474
	13. TYPE OF REPORT & PERIOD COVERED

12. SPONSORING AGENCY NAME AND ADDRESS	Contractor Report
National Aeronautics and Space Administration Washington, D.C. 20546	14. SPONSORING AGENCY CODE

15. SUPPLEMENTARY NOTES

Contract Monitor: Mr. John Kaufman, Atmospheric Science Division, Code ED42, Marshall Space Flight Center, AL 35812

16. ABSTRACT

The effect of a planetary-scale, wavenumber 2 topography on baroclinically active disturbances is investigated for a channel domain in a two-layer, quasi-geostrophic context. When the lower-layer zonal velocity is nonzero, the topography influences the disturbances by forcing a stationary wave, and the topography and the forced wave influence the growth rates and the spatial structures of the time-dependent solutions. The case of zero zonal velocity in the lower layer was also investigated, for which no forced wave exists. Asymptotic forms of the equations, valid when the topographic effect (governed by the ratio of the nondimensional topographic height to the rotational Froude number) is small, are used to obtain both the stationary and time-dependent solutions. The time-dependent solutions are also obtained using a numerical approach, in which is determined the eigenvalues and eigenfunctions of a matrix representing the dynamical equations. Agreement is good between the two approaches.

Recent laboratory experiments by Li, Kung, and Pfeffer, with a baroclinic annulus in which there is a false bottom with wavenumber 2 topography, are used to select governing parameters. The simultaneous presence of a stationary forced wave of wavenumber 2 and a time-dependent baroclinic wave of wavenumber 4, which has wavenumber 2 and 6 sidebands due to the topography, yields a flow field that exhibits some principal features of the laboratory experiments. The position of the forced wave and the location of an excursion in latitude of the storm track show qualitative resemblance to those features observed in the atmosphere.

17. KEY WORDS	18. DISTRIBUTION STATEMENT
Baroclinic Instability Topographic Forcing Rotating Annulus Experiments Storm Tracks	Unclassified - Unlimited Subject Category: 47

19. SECURITY CLASSIF. (of this report)	20. SECURITY CLASSIF. (of this page)	21. NO. OF PAGES	22. PRICE
Unclassified	Unclassified	100	A05

For sale by National Technical Information Service, Springfield, Virginia 22161

NASA-Langley, 1987